Solute dispersion for stable density-driven flow in randomly heterogeneous porous media

Aronne Dell'Oca[1], Monica Riva[1,2], Jesus Carrera[3], Alberto Guadagnini[1,2]

[1]Dipartimento di Ingegneria Civile e Ambientale, Politecnico di Milano, Piazza L. Da Vinci 32, 20133 Milano, Italy

[2]Department of Hydrology and Atmospheric Sciences, University of Arizona, Tucson, AZ 85721, USA

[3] GHS UPC-CSIC, IDAEA, CSIC, Barcelona, 08034, Spain

Correspondence to: aronne.delloca@polimi.it

Keywords: density driven flow; upscaling; dispersive flux; heterogeneity; perturbation expansion.

Abstract

We present a theoretical investigation on the processes underpinning the reduced longitudinal spreading documented in stable variable density flows, as opposed to constant density settings, within heterogeneous porous media. We do so by decomposing velocity and pressure in terms of stationary and dynamic components. The former corresponds to the solution of the constant density flow problem, while the latter accounts for the effects induced by density variability. We focus on a stable flow configuration and analyze the longitudinal spread of saltwater injected from the bottom of a column formed by a heterogeneous porous medium initially fully saturated by freshwater. We adopt a perturbation expansion approach and derive the equations satisfied by section-averaged concentrations and their ensemble mean values. These formulations are respectively characterized by a *single realization* and an *ensemble* dispersive flux, which we determine through appropriate closure equations. The latter are solved via semi-analytical and numerical approaches. Our formulations and associated results enable us to discriminate the relative impact on the density-driven solute displacement of (*a*) covariance of the permeability of the porous medium, (*b*) cross-covariance between permeability and concentration, which is in turn linked to the coupling of flow and transport problems, and (*c*) cross-covariance between the dynamic and stationary velocities.

1. Introduction

Proper understanding and quantification of the feedback between space-time variability of fluid density and the ensuing flow and transport settings is relevant for a variety of environmental and industrial problems. These include, e.g., coastal aquifer management (e.g., [1, 18, 29, 36, 51, 62, 51]), enhanced oil recovery strategies (e.g., [21, 27, 56]), design and engineering of safe CO_2 storage protocols (e.g., [19, 40, 48, 65]) as well as quantification of solute transport in fractured media for site remediation and/or groundwater source protection (e.g., [8, 53, 57]). In this framework, the effect of density contrasts between miscible fluids has been shown to influence the spreading of contaminants along directions parallel (e.g., [13], [24], [39], [66]) and normal to mean flow velocity (e.g., [2, 22, 38, 46, 45, 47, 55, 61, 64]). A notable feature is that settings associated with variable density are characterized by reduced spreading (when compared to constant density) for stable configurations (where the light fluid lies above the dense fluid), and by enhanced spreading for unstable configurations.

Reduced spreading is typically attributed to the occurrence of stabilizing effects. A local increase in velocity causes a perturbation in the concentration front that does not affect velocities in constant density settings. However, the ensuing density increase tends to drag the fluid, resulting in a reduction of the velocity peak and of the overall spreading of concentrations. The results of this stabilizing effect have been documented in nearly homogenous (e.g., [28, 30, 59]) as well as in heterogeneous (e.g., [9, 34, 35, 37]) porous media.

The complexity of the pore scale geometry and flow patterns, which lead to spatial variability of permeability at the continuum scale (e.g., [6, 63]), ultimately governs the variability of solute concentration fields typically observed in natural porous formations (e.g., [50, 56]). A common practice to address this complexity in constant density scenarios relies on decomposing the velocity and concentration fields in terms of the sum of a mean value and a zero-mean fluctuation (i.e., a classical perturbation approach). This decomposition is non-unique and can be performed by considering spatial (e.g., [3, 15, 49, 63]), temporal (e.g., [6, 17]) or ensemble (e.g., [12, 41, 42, 43,

44]) averaging techniques. Regardless the nature of this decomposition, a key research goal is the formulation and solution of an effective model satisfied by a representative (mean/average) concentration. A dispersive flux, given by the average of the cross product between velocity and concentration fluctuations, typically arises in such effective models.

Here, we focus on the interaction between the effects of (*a*) buoyancy and (*b*) heterogeneity induced by the spatial variability of permeability on density-dependent flow and transport behavior. Our key aim is to provide a physically-based quantitative analysis of the above documented reduction of the width of the dispersion zone in stable flow configurations. The essence of the matter is illustrated in Figure 1, obtained using the procedures described in Section 2. Saltwater is continuously injected within a porous domain initially saturated with freshwater. The permeability of the porous medium is modelled as a random function of space characterized by a multivariate log-Gaussian distribution. A realization of permeability is displayed in Figure 1a. Figures 1b, 1c, and 1d display a snapshot of solute concentration, for three diverse values of density contrast, as quantified through the gravity number, N_g, which reflects the relative importance of buoyancy and viscous forces (see Section 2.1 for additional details). These plots evidence two major elements: (*a*) the progressive reduction of the width of the dispersion zone and (*b*) the tendency of the concentration profile to resemble a configuration typical of homogenous media for increasing values of N_g. It is then natural to ask: (*a*) Can we detect the basic physical mechanisms at the heart of this behavior? (*b*) What is the feedback between the effects of buoyancy and physical heterogeneity of the domain in the concentration distribution? and (*c*) Can we quantify the relative importance of buoyancy and permeability heterogeneity on the pattern of the observed spreading process? These are precisely the key questions we address in this work.

Previous studies have adressed the above questions. Hassanizadeh and Lejnse [28] proposed an extension of Fick's law to model the local dispersive flux, i.e., the dispersive flux appearing in the upscaled (from pore- to continuum-scale) transport equation. These authors modeled the local dispersive flux as a nonlinear function of the local concentration gradient through the introduction of

a coefficient of proportionality (termed β by them). This model has been shown to accurately reproduce a set of laboratory experiments in homogenous media under a stable configuration [59], as well as breakthrough curves obtained from a suite of two-dimensional numerical simulations in heterogeneous media, [31]. However, a clear and unambiguous link between β and the underlying physical processes is still missing. Watson et al. [59] and Landman et al. [32] observed that β depends on the mean flow rate. Landman et al. [31] documented a notable dependence of β on the fluid density contrast in heterogeneous formation and introduced two upscaling models (from pore to continuum and from continuum to continuum scale) based on homogenization theory. Both models render a good reproduction of the numerical results of Landman et al. [32] and provide a relatively simple nonlinear relationship between the dispersive flux and the gradient of section averaged concentrations. Welty and Gelhar [60] introduced an analytical expression for the asymptotic (long-time) longitudinal macro-dispersivity under the assumption that the velocity field is a second-order stationary random process. These authors show that macro-dispersion is a function of the gradient of the ensemble mean concentration, flow rate, displacement distance, gravity, fluid density and viscosity and log-permeability correlation scale and variance. However, as we highlight in Section 3, the velocity field is not (statistically) stationary in a variable density problem, due to the coupling between flow and transport equations. In this framework, the objectives of this work are (i) to obtain an upscaled equation for flow and transport in a variable density context, (ii) to highlight the factors that control the dispersive flux, and (iii) to investigate the features of the reduced solute dispersion that is observed under stable displacement conditions.

2. Flow and transport Model and problem set up

Fluid flow in porous media is described by conservation of mass and Darcy's law, in the form

$$\frac{\partial \phi \rho^*}{\partial t^*} + \nabla^* \cdot \left(\rho^* \boldsymbol{q}^* \right) = 0, \qquad \boldsymbol{q}^* = -\frac{\boldsymbol{k}^*}{\mu^*} \cdot \left(\nabla^* p^* + \rho^* g^* \nabla^* z^* \right), \tag{1}$$

where ρ^* [ML^{-3}], μ^* [M T^{-1} L^{-1}] and p^* [M T^{-2} L^{-1}] are fluid density, viscosity, and pressure,

respectively, g^* [LT^{-2}] is gravity, z^* [L] is elevation, t^* [T] is time, $\boldsymbol{q}^*$ [L T^{-1}] is Darcy's flux, $\boldsymbol{k}^*$ [L^2] is the permeability tensor and ϕ [-] is porosity, which we treat as a constant scalar.

We consider solute transport to be locally governed by the advection-dispersion equation

$$\frac{\partial\left(\phi\rho^* C^*\right)}{\partial t^*}+\nabla^*\cdot\left(\rho^*\boldsymbol{q}^* C^*\right)-\nabla^*\cdot\left(\phi\rho^*\boldsymbol{D}^*\cdot\nabla^* C^*\right)=0\,. \tag{2}$$

Here C^* [-] is solute concentration, and $\boldsymbol{D}^*$ [L T^{-2}] is the local dispersion tensor, modeled as

$$\boldsymbol{D}^*=\left(D_m^*+\alpha_T{}^*\,|\boldsymbol{v}^*|\right)\mathbf{I}+\left(\alpha_L{}^*-\alpha_T{}^*\right)\frac{\boldsymbol{v}^*\boldsymbol{v}^*}{|\boldsymbol{v}^*|}\,, \tag{3}$$

where $D_m{}^*$ is molecular diffusion, $\alpha_T{}^*$ and $\alpha_L{}^*$ [L] respectively are transverse and longitudinal dispersivities, $\mathbf{I}$ is the identity matrix, and $\boldsymbol{v}^*$ [L T^{-1}] is fluid velocity defined as

$$\boldsymbol{v}^*=\boldsymbol{q}^*/\phi\,. \tag{4}$$

We focus on a stable density-dependent problem within a heterogeneous porous domain, Ω, of width W^* [L], and height H^* [L], as depicted in Figure 1. In our set-up Darcy's flux $\boldsymbol{q}^*$ has components q_z^* and q_y^*, respectively along the vertical, z^*, and horizontal, y^*, direction. The column is initially filled by freshwater with density ρ_f^*. Seawater with density ρ_s^* at concentration C_s is continuously injected at time $t^*\geq 0$ at the bottom of the column, i.e., at $z^*=0$. The remaining boundary conditions are: (1) no flow at $y^*=0, W^*$; (2) constant pressure $p^*=p_{BC}^*$ at $z^*=0$; (3) prescribed vertical flux, $q_z^*=q_{BC}^*$, and solute mass flux $\left(\boldsymbol{q}^* C^*-\boldsymbol{D}^*\cdot\nabla^* C^*\right)\cdot\boldsymbol{n}^*=q_{BC}^* C^*$ at $z^*=H^*$, with $\boldsymbol{n}^*$ being a unit vector pointing outwards (see Figure 1).

Closure of the system (1)-(4) is obtained by assuming viscosity to be constant and expressing ρ^* as a linear function of C^* (e.g., [1])

$$\rho^*=\rho_f^*+\beta^* C^*,\quad \text{with } \beta^*=\left(\rho_s^*-\rho_f^*\right)/C_s\,. \tag{5}$$

In the following we assume isotropic dispersivity values, $\alpha_T^* = \alpha_L^* = \alpha^*$ and disregard D_m^* since its contribution to the dispersion tensor can be usually neglected (e.g., [31]). Therefore, (3) reduces to

$$\boldsymbol{D}^* = \alpha^* |\boldsymbol{v}^*| \mathbf{I}. \tag{6}$$

We adopt $\sqrt{\tilde{k}^*}$, k^* being the geometric mean of the permeability field, as characteristic length scale. This leads to the introduction of the following dimensionless quantities

$$\begin{aligned} &y = \frac{y^*}{\sqrt{\tilde{k}^*}}, \quad z = \frac{z^*}{\sqrt{\tilde{k}^*}}, \quad \boldsymbol{k} = \frac{\boldsymbol{k}^*}{\tilde{k}^*}, \quad \boldsymbol{q} = \frac{\boldsymbol{q}^*}{v_{BC}^*}, \quad \boldsymbol{v} = \frac{\boldsymbol{v}^*}{v_{BC}^*}, \quad \nabla = \sqrt{\tilde{k}^*}\nabla^*, \\ &\rho = \frac{\rho^*}{\Delta\rho^*}, \quad p = \frac{p^*}{\mu^* v_{BC}^* / \sqrt{\tilde{k}^*}}, \quad t = \frac{t^*}{\sqrt{\tilde{k}^*} / v_{BC}^*}, \qquad C = \frac{C^*}{C_s}, \end{aligned} \tag{7}$$

with $\Delta\rho^* = \rho_s^* - \rho_f^*$, $v_{BC}^* = q_{BC}^* / \phi$. Using (7), Eqs. (1), (2), (5) and (6) can be written in dimensionless form as

$$\frac{\partial \phi\rho}{\partial t} + \nabla\cdot(\rho\boldsymbol{q}) = 0, \quad \boldsymbol{q} = -\boldsymbol{k}\cdot(\nabla p + \mathrm{N_g}\rho\nabla z), \qquad \text{with } \mathrm{N_g} = \frac{\Delta\rho^* \tilde{k}^* g^*}{\mu^* v_{BC}^*}, \tag{8}$$

$$\frac{\partial(\rho\phi C)}{\partial t} + \nabla\cdot(\rho\boldsymbol{q}C) - \nabla\cdot(\rho\phi\boldsymbol{D}\cdot\nabla C) = 0, \tag{9}$$

$$\rho = \rho_f + C \qquad \text{with } \rho_f = \frac{\rho_f^*}{\Delta\rho^*}, \tag{10}$$

$$\boldsymbol{D} = \frac{|\boldsymbol{v}|}{\mathrm{Pe}}\mathbf{I} \qquad \text{with } \mathrm{Pe} = \frac{\sqrt{\tilde{k}^*}}{\alpha^*}. \tag{11}$$

Here, Pe is the Peclet number, expressing the ratio between advective and dispersive transport rate, and $\mathrm{N_g}$ is the gravity number, expressing the relative intensity of buoyancy and viscosity effects.

We solve (8)-(11) by means of the widely tested code SUTRA [58]. Domain heterogeneity is modeled by treating the dimensionless permeability $\boldsymbol{k}$ as an isotropic random field $\boldsymbol{k} = \exp(Y(y,z))\mathbf{I}$, where $Y(y, z)$ is a zero-mean second order stationary random process of space characterized by an isotropic exponential covariance function

$$C_{YY}(\boldsymbol{r}^*) = \sigma_Y^2 \exp(-|\boldsymbol{r}^*|/l^*), \quad (12)$$

$\boldsymbol{r}^*$ [L], σ_Y^2 [-] and l^* [L] respectively being the separation vector (or lag) between two spatial locations, variance and correlation length (or integral scale) of Y. The heterogeneous Y fields are synthetically generated by the widely used and tested code SGSIM [20] on a uniform grid structured with five generation nodes per correlation length, l^* as detailed in Section 4.

3. Theoretical framework

We start by deriving the equation satisfied by section-averaged concentrations in the setting of Figure 1, which naturally leads to an effective one-dimensional model. This equation includes a term, called *single realization* dispersive flux, which enables us to embed in a simple one-dimensional (along the mean flow direction) mathematical formulation the effect of the spatial heterogeneity of $\boldsymbol{k}$. We then leverage on the above one-dimensional (section-averaged) model and average it in probability space. The ensuing mathematical formulation includes an *ensemble* dispersive flux that enables us to encapsulate the effect of the uncertainty in the spatial arrangement of $\boldsymbol{k}$ on the mean concentration distribution. The main purpose of the analytical formulations presented in Sections 3.1-3.2 is to enrich our understanding of the interplay between permeability and stabilizing effects that is at the origin of the solute spread reduction taking place in stable flows within heterogeneous media. Our formulations facilitate grasping the impact of variations of N_g and σ_Y^2 on the system behavior in terms of flow structure and resulting solute spreading. Our study enables us to link the key moments of the flow and log-permeability fields to the solute spreading behavior.

3.1 Section-Averaged Concentration

Point concentration values $C(y,z,t)$ are seldom available from laboratory or field experiments [7], section-averaged concentration profiles being typically monitored (e.g., [11, 23, 26, 31, 39, 52]). Therefore, we focus on cross-section (or horizontal) average concentration, $\overline{C}(z,t)$, where the overbar indicates the horizontal averaging operator defined as

$$\overline{\Theta} = \frac{1}{W}\int_0^W \Theta(y)dy\,, \tag{13}$$

where Θ denotes a generic quantity (a parameter or a state variable). In the following, we derive the equation satisfied by $\overline{C}(z,t)$ relying on the Boussinesq approximation (e.g., [18], [21]), i.e., assuming that $\nabla\cdot\boldsymbol{q} >> \frac{\phi}{\rho}\frac{\partial\rho}{\partial t} + \boldsymbol{q}\cdot\frac{\nabla\rho}{\rho}$. Under this assumption (8) and (9) can be simplified as

$$\nabla\cdot\boldsymbol{v} = 0, \qquad \boldsymbol{q} = -\boldsymbol{k}\cdot\left(\nabla p + \mathrm{N_g}\rho\nabla z\right), \tag{14}$$

$$\frac{\partial C}{\partial t} + \boldsymbol{v}\cdot\nabla C - \nabla\cdot\left(\boldsymbol{D}\cdot\nabla C\right) = 0\,. \tag{15}$$

Note that $\boldsymbol{k}$ is spatially variable and all remaining quantities (i.e., $\boldsymbol{v}$, $\boldsymbol{q}$, p, ρ, C and $\boldsymbol{D}$) are both spatially and temporally variable. According to (14)-(15), steady state conditions never occur in the variable density problem considered in this work and sketched in Figure 1 because flow evolves in time due to the effects of the buoyancy term in (14). Therefore, (14) must be solved jointly with (10) and (15).

We decompose each variable in (14)-(15) as the sum of a horizontal spatial mean and a (spatial) zero-mean fluctuation (along the *y*-direction), i.e.,

$$\begin{aligned} &p = \overline{p} + p', && C = \overline{C} + C', && \boldsymbol{k} = \mathbf{I} + k'\mathbf{I}, \\ &\rho = \overline{\rho} + \rho', && \boldsymbol{v} = \overline{\boldsymbol{v}} + \boldsymbol{v}', && \boldsymbol{D} = \overline{\boldsymbol{D}} + \boldsymbol{D}', \end{aligned} \tag{16}$$

where horizontally-averaged quantities depend on (z,t), while fluctuations depend on (y,z,t). According to (10), one can see that

$$\overline{\rho} = \rho_f + \overline{C}, \qquad \rho' = C'\,. \tag{17}$$

Horizontally averaged concentrations, $\overline{C}(z,t)$, satisfy the following equation (see A.4 in Appendix A)

$$\frac{\partial\overline{C}}{\partial t} + \frac{\partial\overline{C}}{\partial z} - \frac{1}{\mathrm{Pe}}\frac{\partial^2\overline{C}}{\partial z^2} + \frac{\partial\overline{v_z'C'}}{\partial z} = 0\,, \tag{18}$$

where $\overline{v_z'C'}$ is the *single realization* dispersive flux. At second order, the latter reads (see A.11a)

$$\overline{v_z'C'} = -\int_0^t \int_0^H \overline{v_z'(z,t)v_z'(\xi,\tau)}\, G_z^T(z,t,\xi,\tau)\frac{\partial \overline{C}(\xi,\tau)}{\partial \xi} d\xi d\tau \,. \tag{19}$$

Here, $G_z^T(z,t,\xi,\tau)$ is the deterministic Green's function introduced in (A.10) and $\overline{v_z'(z,t)v_z'(\xi,\tau)}$ (defined in (A.11b)) is the horizontal average of $v_z'(y,z,t)v_z'(\eta = y,\xi,\tau)$, i.e., of the product between vertical velocity fluctuations evaluated at the same horizontal coordinate and diverse vertical positions and times. The single realization dispersive flux, $\overline{v_z'C'}$, embeds in the upscaled one-dimensional (vertical) model (18) the effect of permeability fluctuations on the section-averaged concentration $\overline{C}(z,t)$ (e.g., [16]).

To highlight the effect of density variations on $C(y,z,t)$, we decompose the vector of velocity fluctuations as the sum of (*a*) a *stationary* component, $\boldsymbol{v}^{st}'(z,y)$, which corresponds to the solution of (14) with constant density ($\rho = \rho_f$), and (b) a *dynamic* component, $\boldsymbol{v}^{dy}'(z,y,t)$, accounting for the stabilizing buoyancy effects due to density variations, i.e.,

$$\boldsymbol{v}'(y,z,t) = \boldsymbol{v}^{st}'(y,z) + \boldsymbol{v}^{dy}'(y,z,t)\,. \tag{20}$$

The equations satisfied by $\boldsymbol{v}^{st}'(y,z)$ and $\boldsymbol{v}^{dy}'(y,z,y)$ are derived in Appendix C and read (see (C.5))

$$v_z^{st}'(y,z) = Y(y,z) - \frac{1}{\phi}\frac{\partial p^{st}'(y,z)}{\partial z}, \qquad v_z^{dy}'(y,z,t) = -\frac{1}{\phi}\left(\frac{\partial p^{dy}'(y,z,t)}{\partial z} + \mathrm{N_g}\,\rho'(y,z,t)\right), \tag{21}$$

Here, similar to (20), we decompose pressure fluctuation $p'(y,z,t)$ as the sum of a *stationary*, $p^{st}'(y,z)$, and a *dynamic*, $p^{dy}'(y,z,t)$, component. A numerical analysis of (21) (details not shown) reveals that, for the set up of Figure 1, $Y(y,z) >> \partial p^{st}'(y,z)/\partial z/\phi$ and $\mathrm{N_g}\,\rho'(y,z,t) >> \partial p^{dy}'(y,z,t)/\partial z$. Therefore, (21) can be approximated as

$$v_z^{st}'(y,z) \approx Y(y,z)\ , \qquad v_z^{dy}'(y,z,t) \approx -\frac{\mathrm{N_g}}{\phi}\rho'(y,z,t)\,. \tag{22}$$

While (22) shows a clear dependence of $v_z^{st}'(y,z)$ on the fluctuation $Y(y,z)$ of the permeability field,

the behavior of $v_z^{dy}{}'(y,z,t)$ depends on that of $\rho'(y,z,t)$ through the multiplying factor $\mathrm{N_g}/\phi$. Noticing that according to (17) $\rho'(y,z,t)=C'(y,z,t)$, and making use of (20) and (A.8), the second of (22) can be rewritten as

$$v_z^{dy}{}'(y,z,t)\approx-\frac{\mathrm{N_g}}{\phi}C'(z,y,t)=\frac{\mathrm{N_g}}{\phi}\int_0^t\int_\Omega\left[Y(\eta,\xi)-\frac{\mathrm{N_g}}{\phi}\rho'(\eta,\xi,\tau)\right]\frac{\partial\bar{C}(\xi,\tau)}{\partial\xi}G^T(y,z,t;\xi,\eta,\tau)d\eta d\xi d\tau \tag{23}$$

Equation (23) allows recognizing that $v_z^{dy}{}'(y,z,t)$ is a non-local quantity embedding flow and transport features. Two effects are encapsulated in (23): (*i*) permeability fluctuations are seen to promote velocity fluctuations; (*ii*) the action of the stabilizing buoyant term contributes to reducing velocity fluctuations, with an intensity proportional to $\mathrm{N_g}$ and to the density fluctuations. These two competing mechanisms are weighted by the mean concentration (or density) gradient, the behavior of which is a function of both $\mathrm{N_g}$ and permeability heterogeneity.

In the following, we briefly elucidate the benefit of decomposition (20) by focusing on a simple heterogeneous domain formed by a single semi-circular inclusion of high permeability $\boldsymbol{k}(y,z)=10\mathbf{I}$ (depicted in red in Figures 2*a*-2*c*), within an otherwise uniform porous medium with $\boldsymbol{k}(y,z)=\mathbf{I}$. The remaining relevant key dimensionless quantities are set to $\mathrm{N_g}=0.35$, $\mathrm{Pe}=0.25$, $\phi=0.35$, $\rho_f=40$. The analysis for randomly heterogeneous porous media is offered in Section 4. Figures 2*a*, 2*b* and 2*c* respectively depict $\boldsymbol{v}^{st}{}'(y,z)$, $\boldsymbol{v}^{dy}{}'(y,z,t)$ and $\boldsymbol{v}'(y,z,t)$ at time t = 664. The total velocity field $\boldsymbol{v}(y,z,t)$ is shown in Figure 2*d* together with the concentration field. As an additional term of comparison, Figure 2*e* depicts $\boldsymbol{v}(y,z)$ and $C(y,z,t)$ computed at the same dimensionless time considering a solute with $\rho=\rho_f$ (i.e., corresponding to the transport of a passive scalar in a constant density setting). Figures 2*d* and 2*e* clearly show that solute spreading decreases when density effects are considered. This observed reduction of solute dispersion for the variable density stable scenario is strictly linked to the ensuing velocity distribution. Figure 2*a* indicates that vertical *stationary* flow

fluctuations, $v_z^{st}{}'$, are positive in the high permeability zone, favoring solute advancement within this area. This generates positive density fluctuations, ρ', which in turn trigger negative vertical *dynamic* flow fluctuations, $v_z^{dy}{}'$, due to the effect of (reduction in) buoyancy (see Figure 2*b*). The opposite occurs in the portion of the domain adjacent to the high permeability inclusion. Since $v_z^{st}{}'$ and $v_z^{dy}{}'$ are associated with opposite signs, the total vertical flow fluctuation v_z' is smaller than its counterpart evaluated for the constant density scenario (compare Figure 2*c* and Figure 2*a*). Note that the stabilizing effect of $v_z^{dy}{}'$ tends to decrease the intensity of v_z' (with respect to the uniform density case) without altering its sign. This behavior is also observed in the heterogeneous field analyzed in Section 4 for the investigated values of N_g. Ultimately, the velocity field at the solute front is more uniform in the variable density than in the constant density case (compare the velocity fields in Figures 2*d* and 2*e*) causing a decreased solute dispersion in the former scenario, as compared against the latter. This observation is further supported by Figures 2*f* and 2*e* where the distribution along *z* of the variance of the vertical velocity, $\overline{\sigma}_{v_z}^2(z,t)$, and of $\overline{v_z'C'}$ (19) for the constant density case (black curves) are compared against their counterpart associated with variable density (red curves). One can clearly note the reduction of the magnitude of both $\overline{\sigma}_{v_z}^2(z,t)$ and $\overline{v_z'C'}$ under variable density conditions. The basic mechanisms highlighted here for this relatively simple heterogeneous configuration are at the heart of the observed reduction in solute spreading observed for stable variable density flow within heterogeneous porous media, as further discussed in Section 4.

3.2 Ensemble Analysis

Here we treat $\boldsymbol{k}$ as a second order stationary random field and derive the equation satisfied by the ensemble mean of the section-averaged concentration, i.e., $\left\langle \overline{C}(z,t) \right\rangle$, $\langle\ \rangle$ indicating the ensemble mean operator. This analysis enables us to link the main features of $\left\langle \overline{C}(z,t) \right\rangle$ to key statistics of the permeability field. The equation satisfied by $\left\langle \overline{C}(z,t) \right\rangle$ results from ensemble averaging of (18), i.e.,

$$\frac{\partial\langle\bar{C}\rangle}{\partial t}+\frac{\partial\langle\bar{C}\rangle}{\partial z}-\frac{1}{\mathrm{Pe}}\frac{\partial^2\langle\bar{C}\rangle}{\partial z^2}+\frac{\partial\langle\overline{v_z'C'}\rangle}{\partial z}=0, \tag{24}$$

where $\langle\overline{v_z'C'}\rangle$ is the *ensemble* dispersive flux defined, at second order and after localization with respect to the mean concentration vertical gradient, as (see Appendix B, eq. (B.3))

$$\langle\overline{v_z'C'}\rangle=-\int_0^t\int_0^H\langle\overline{v_z'(z,t)v_z'(\xi,\tau)}\rangle G_z^T(z,t,\xi,\tau)d\xi d\tau\frac{\partial\langle\overline{C}(z,t)\rangle}{\partial z}. \tag{25}$$

Here $\langle\overline{v_z'(z,t)v_z'(\xi,\tau)}\rangle$ is the horizontal spatial mean of $\langle v_z'(y,z,t)v_z'(\eta=y,\xi,\tau)\rangle$ which is the covariance between the vertical velocity fluctuation at *z* at time *t* and its counterpart evaluated at ξ at time τ, both at the same horizontal coordinate *y*. The *ensemble* dispersive flux takes into account the effect of the spatial heterogeneity of ***k*** across the *ensemble* of realizations on the evaluation of the *ensemble* mean of the section-averaged concentration. As discussed by Morales-Casique et al. [41], [42], the *ensemble* dispersive flux is related to the effects of the loss of information associated with the random nature of ***k***, and therefore of the velocity field, on the prediction of C through $\langle\bar{C}\rangle$.

Equation (25) highlights the key role of the velocity field statistics in controlling the ensemble dispersive flux. We show in Appendix D that the velocity covariance, $\langle\overline{v_z'(z,t)v_z'(\xi,\tau)}\rangle$, can be decomposed as the sum of four terms, involving stationary and dynamic velocity fluctuations, as (see (D.12))

$$\begin{aligned}\langle\overline{v'_z(z,t)v'_z(\xi,\tau)}\rangle&=\langle\overline{v_z^{st}'(z)v_z^{st}'(\xi)}\rangle+\langle\overline{v_z^{st}'(z)v_z^{dy}'(\xi,\tau)}\rangle+\langle\overline{v_z^{dy}'(z,t)v_z^{st}'(\xi)}\rangle+\langle\overline{v_z^{dy}'(z,t)v_z^{dy}'(\xi,\tau)}\rangle\\&=\mathbf{A}\{\langle\overline{Y(z)Y(\xi)}\rangle\}+\frac{\mathrm{N_g}}{\phi}\mathbf{B}\{\langle\overline{Y(z)C'(\xi,\tau)}\rangle\}+\frac{\mathrm{N_g}}{\phi}\mathbf{C}\{\langle\overline{C'(z,t)Y(\xi)}\rangle\}+\frac{\mathrm{N_g^2}}{\phi^2}\mathbf{D}\{\langle\overline{C'(z,t)C'(\xi,\tau)}\rangle\}\end{aligned}, \tag{26}$$

where $\mathbf{A}\{\ \}$, $\mathbf{B}\{\ \}$, $\mathbf{C}\{\ \}$, $\mathbf{D}\{\ \}$ are operators defined (D.8)-(D.11). Equation (26) indicates that while the horizontal spatial mean of the *stationary-stationary* term, $\langle\overline{v_z^{st}'(z)v_z^{st}'(\xi)}\rangle$, depends on the

covariance of the log-permeability field, the *stationary-dynamic*, $\left\langle \overline{v_z^{st}{}'(z)v_z^{dy}{}'(\xi,\tau)} \right\rangle$, and *dynamic-stationary*, $\left\langle \overline{v_z^{dy}{}'(z,t)v_z^{st}{}'(\xi)} \right\rangle$, terms depend on the cross-covariance $\left\langle \overline{Y(z)C'(\xi,\tau)} \right\rangle$ between log permeability and concentration and are characterized by a quasi-linear dependence on N_g, since $\left\langle \overline{Y(z)C'(\xi,\tau)} \right\rangle$ in (26) depends on N_g as dictated by (E.5). Otherwise, the *dynamic-dynamic* component, $\left\langle \overline{v_z^{dy}{}'(z,t)v_z^{dy}{}'(\xi,\tau)} \right\rangle$, is a function of the covariance of the concentration field, $\left\langle \overline{C'(z,t)C'(\xi,\tau)} \right\rangle$, and exhibits a quasi-linear dependence on N_g^2 (note that also $\left\langle \overline{C'(z,t)C'(\xi,\tau)} \right\rangle$ depends on N_g, as shown in (F.6)). The main features of covariances embedded in (26) and their impact on the solute transport behavior are analyzed and discussed in Section 4. Note that the constant flow boundary condition and the adoption of the Boussinesq approximation in our set-up ensure that the center of mass of the advancing solute front travels at the same speed for all realizations of *Y*, thus yielding no artificial spreading (see e.g., [16]).

4. Results and discussion

Numerical Monte Carlo (MC) based and semi-analytical results are presented here for the quantities introduced in Section 3, i.e., velocity covariance, cross-covariance between concentration and permeability, ensemble dispersive flux and concentration variance. Numerical and semi-analytical results are depicted as solid and dashed curves, respectively, in the plots of this Section. We recall for convenience the main assumptions invoked in our semi-analytical formulations presented in Section 3, i.e.,: (*i*) all statistical moments are approximated at second order (in terms of the fluctuation *Y* of the permeability field), thus nominally limiting our semi-analytical solution to mildly heterogeneous media, $\sigma_Y^2 << 1$; (*ii*) flow and transport Green's functions are approximated by their one-dimensional formulations (A.10) and (D.4b). Additionally, to speed up the evaluation of our semi-analytical expressions and to make use of already existing analytical results, (*iii*) cross-covariance between log conductivity and hydraulic head in (E.5) is computed via an analytical

solution available for mean uniform steady-state flow in an infinite two-dimensional domain [14]; and (*iv*) the contribution of $\left\langle \overline{v_z^{st}'(z) v_z^{st}'(\xi)} \right\rangle$ in (25)-(26) is set equal to $\sigma_Y^2 l$, which corresponds to the asymptotic value for macro dispersion derived in Gelhar and Axness [25]. Due to the coupled nature of the problem (e.g., $\left\langle \overline{v_z' C'} \right\rangle$ depends on $\partial \left\langle \overline{C} \right\rangle / \partial z$, as shown by (24)), a semi-analytical solution for the quantities presented in Section 3 requires an iterative procedure and therefore a CPU time which is comparable with the one associated with MC simulations. Hence, in the following we take advantage of the MC results to evaluate the mean concentration gradient, $\partial \left\langle \overline{C} \right\rangle / \partial z$.

In our simulations we set $\phi = 0.35$, k^* = 10^{-9} m^2, H^* = 0.3 m, W^* = 0.05 m, α^* = 1.25×10^{-4} m, $\rho_f^* = 1000$ kg / m^3, $\rho_s^* = 1025$ kg / m^3, l^* = 2.50×10^{-3} m (i.e., $H^* / W^* = 6$, $H = H^* / \sqrt{k^*} \approx 9486.8$, $W = W^* / \sqrt{k^*} \approx 1581.1$, $l = l^* / \sqrt{k^*} = 79$, $H^* / l^* = 120$, $W^* / l^* = 20$, Pe = 0.25, $l^* / \alpha^* = 20$, $\rho_f = 40$). The size of the domain has been selected to ensure that we frame our calculations on a large system, in terms of the correlation scale, l^*, of *Y*. The domain is discretized by a regular mesh of square elements. We performed a set of preliminary simulations aimed at testing the influence of space and time grid discretization on the quantities of interest (namely, horizontal mean concentration, *single realization* and *ensemble* dispersive flux and velocity covariance). Accurate results at an affordable CPU time have been obtained with a spatial grid formed by 100 × 600 elements (i.e., $\Delta z^* = \Delta y^*$ = 5×10^{-4} m) and dimensionless time step Δt = 2.8. Five rows of grid elements formed by a homogeneous porous medium with $k^* = k^*$ are added at the inlet boundary to regularize solute inflow. This procedure is commonly adopted in experimental set-ups with highly heterogeneous porous media (e.g., Kretz et al., 2003) to regularize the inflow conditions. We investigate four scenarios characterized by diverse levels of heterogeneity of the permeability field, i.e., σ_Y^2 = 0.1,

0.5, combined with diverse intensities of buoyancy effects, as quantified by N_g = 0, 0.1, 1.0. Our numerical results are grounded on 1000 MC simulations for each parameter set investigated.

4.1 Variance and Covariance of Vertical Velocity

The covariance of the vertical velocity components (26) plays a critical role in determining the mean solute transport behavior, as highlighted by (24)-(25). Here, we compare the results obtained for the constant and variable density scenarios to elucidate and quantify the origin of the reduced solute spreading documented in Figure 1.

Figures 3 depicts the velocity variance, $\left\langle \overline{v_z'^2} \right\rangle$, and the (negative) mean concentration gradient, $-\partial \left\langle \overline{C} \right\rangle / \partial z$, at three dimensionless times (i.e., $t_1 = 2.2\times10^3$, $t_2 = 4.4\times10^3$, and $t_3 = 6.6\times10^3$) for $N_g = 1$ (left) and $N_g = 0.1$ (right) and for $\sigma_Y^2 = 0.1$ (two top rows) and $\sigma_Y^2 = 0.5$ (two bottom rows). For illustration purposes, Figure 3 includes only the Monte Carlo based numerical results. The corresponding semi-analytical results are in good agreement with these. Velocity variance $\left\langle \overline{v_z'^2} \right\rangle$ varies with *z*. It is zero at the boundaries (recall that we maintain a constant permeability at the five extreme rows of elements), but immediately rises to its constant density stationary value, except at the region near the solute front, where it is reduced. This reduction reflects the role of the space-time variability of fluid density in stabilizing the system, thus reducing $\left\langle \overline{v_z'^2} \right\rangle$ at the solute front as N_g increases. The occurrence of local minima of $\left\langle \overline{v_z'^2} \right\rangle$ and $\partial \left\langle \overline{C} \right\rangle / \partial z$ is strikingly evident for $N_g = 1$ and small heterogeneity ($\sigma_Y^2 = 0.1$). Decreasing the intensity of buoyancy effects (i.e., for $N_g = 0.1$) and/or increasing σ_Y^2 cause the local minima of $\left\langle \overline{v_z'^2} \right\rangle$ to be dampened and local maxima of $-\partial \left\langle \overline{C} \right\rangle / \partial z$ to decrease. We remark that there is strong feedback between the behavior of $\left\langle \overline{v_z'^2} \right\rangle$ and $\partial \left\langle \overline{C} \right\rangle / \partial z$. An increase of $\left\langle \overline{v_z'^2} \right\rangle$ and the corresponding increase of the vertical velocity fluctuation

$v_z'(y,z,t)$ is associated with an increase of the solute spreading. These are in turn linked to a decrease of the mean concentration gradient, $\partial\langle\overline{C}\rangle/\partial z$, i.e., to a smoothing of mean concentration profiles.

We have shown in (26) that the vertical velocity covariance, $\langle\overline{v_z'(z,t)v_z'(\xi,\tau)}\rangle$, can be decomposed as the sum of four components. These are shown in Figure 4 for $\sigma_Y^2 = 0.1$, and $N_g = 1$ (left) and $N_g = 0.1$ (right). Both the overall covariance $\langle\overline{v_z'(z,t)v_z'(\xi,\tau)}\rangle$ (red curve Figure 4a) and its stationary component $\langle\overline{v_z^{st}'(z)v_z^{st}'(\xi)}\rangle$ (black curve) attain their maximum value at the front (the curves are plotted versus ξ for fixed $t=\tau=t_2$ and $z=z_2=4.27\times10^3$). Obviously, this maximum is the variance, which was shown (Figure 3(a) and (b)) to display a minimum at the front for the variable density case. The reduction in variance is now manifest (Figures 4(a) and (b)) in the observation that the peak displayed by $\langle\overline{v_z'(z,t)v_z'(\xi,\tau)}\rangle$ at $\xi = z$ is smaller than that of $\langle\overline{v_z^{st}'(z)v_z^{st}'(\xi)}\rangle$. A perhaps more interesting effect is the asymmetry introduced by variable density on the velocity covariance, which is symmetric and positive for constant density. In fact, $\langle\overline{v_z'(z,t)v_z'(\xi,\tau)}\rangle$ and $\langle\overline{v_z^{st}'(z)v_z^{st}'(\xi)}\rangle$ tend to coincide for $\xi > z$; but $\langle\overline{v_z'(z,t)v_z'(\xi,\tau)}\rangle$ becomes significantly smaller, even negative, than $\langle\overline{v_z^{st}'(z)v_z^{st}'(\xi)}\rangle$ for $\xi \le z$. As expected, $\langle\overline{v_z'(z,t)v_z'(\xi,\tau)}\rangle$ and $\langle\overline{v_z^{st}'(z)v_z^{st}'(\xi)}\rangle$ tend to coincide when N_g decrease (see Figure 4*b*).

Negative values of the overall covariance $\langle\overline{v_z'(z,t)v_z'(\xi,\tau)}\rangle$ for $\xi \le z$ are due to the effect of the *dynamic* and *stationary* velocity cross-covariances, $\langle\overline{v_z^{dy}'(z,t)v_z^{st}'(\xi)}\rangle$ and $\langle\overline{v_z^{st}'(z)v_z^{dy}'(\xi,\tau)}\rangle$, which are always negative. This result is consistent with (23) and with our discussion in Section 3 arguing that positive values of $v_z^{st}'(\xi)$ favor the solute to advance within the domain, thus originating negative *dynamic* velocity fluctuations, $v_z^{dy}'(z\ge\xi,t)$, through positive density fluctuations, $\rho'(z\ge\xi,t)$. The

same holds when $v_z^{st}'(\xi)$ is negative, which promotes positive values of $v_z^{dy}'(z \geq \xi, t)$. We note that $\left\langle \overline{v_z^{dy}'(z,t) v_z^{st}'(\xi)} \right\rangle$ attains its largest (absolute) value for $\xi < z$ and $\left\langle \overline{v_z^{st}'(z) v_z^{dy}'(\xi,\tau)} \right\rangle$ for $\xi > z$. These findings suggest that the stabilizing *dynamic* fluctuation $\left\langle \overline{v_z^{dy}'(z,t) v_z^{st}'(\xi)} \right\rangle$ arising at a given space-time location (z, t) displays a strong negative correlation with the *stationary* velocity fluctuations (i.e., with variations of Y according to (22)), especially those occurring at points $\xi < z$. This is a result of (*i*) the coupling between flow and transport (as documented by the dependency of v_z^{dy}' on ρ' in (22) and (23)), and (*ii*) the nature of the transport setting according to which density fluctuations are mainly dictated by the velocity perturbations which have been already experienced. This aspect is clearly highlighted by our semi-analytical solution (23) since the Green's function (A.10) of the transport problem is non zero mainly in the range of space-time coordinates $(\xi \leq z; \tau \leq t)$. As a consequence, fluctuations v_z^{dy}', which are rooted in the coupled nature of flow and transport, are less correlated with the corresponding *stationary* flow perturbation, v_z^{st}', which occur at forward (in space and time along the mean flow direction) locations. The term $\left\langle \overline{v_z^{dy}'(z,t) v_z^{st}'(\xi)} \right\rangle$ depicted in Figure 4*c*-4*d* imbues information about the extent of the region within which the *dynamic* velocity field at a given location (in space-time) is influenced by variation of the *stationary* velocity field at all locations within the domain. At the same time, $\left\langle \overline{v_z^{st}'(z) v_z^{dy}'(\xi,\tau)} \right\rangle$ depicted in Figures 4*e*-4*f* can be seen as an indication of the extent in space and time of the region within which *stationary* velocity fluctuations promote *dynamic* perturbations of the flow, an effect which is mainly felt at spatial locations $\xi > z$. In other words, while Figures 4*c*-4*d* highlight the way density (or concentration) perturbations at a given location are affected by the heterogeneity spanning the entire domain, Figures 4*e*-4*d* highlight the way a local perturbation of the log permeability field contributes to the concentration variability

across the full domain. Note also that a change in N_g induces a quasi-linear variation of the magnitude of $\left\langle \overline{v_z^{st}{}'(z) v_z^{dy}{}'(\xi,\tau)} \right\rangle$ and $\left\langle \overline{v_z^{dy}{}'(z,t) v_z^{st}{}'(\xi)} \right\rangle$, as also indicated by (26).

Figures 4*g* and 4*h* depict $\left\langle \overline{v_z^{dy}{}'(z,t) v_z^{dy}{}'(\xi,\tau)} \right\rangle$ versus ξ for $z = z_2$, $t = t_2$ and three values of τ when $N_g = 1$ and 0.1, respectively. This quantity represents the covariance between the *dynamic* velocity components, which is positive, as expected. It can then be noted that $\left\langle \overline{v_z^{dy}{}'(z,t) v_z^{dy}{}'(\xi,\tau)} \right\rangle$ exhibits a supra-linear dependence on N_g, with a power which is different from two (compare Figures 4*g* and 4*h*) according to (26) and (F.6). Quantities $\left\langle \overline{v_z^{dy}{}'(z,t) v_z^{st}{}'(\xi)} \right\rangle$, $\left\langle \overline{v_z^{st}{}'(z) v_z^{dy}{}'(\xi,\tau)} \right\rangle$ and $\left\langle \overline{v_z^{dy}{}'(z,t) v_z^{dy}{}'(\xi,\tau)} \right\rangle$ display a behavior which is qualitatively similar to what illustrated above at all space-time locations investigated (details not shown).

Figure 5 depicts results analogous to those of Figure 4 for $\sigma_Y^2 = 0.5$. For both Y variances, the semi-analytical solution captures remarkably the behavior of the Monte Carlo results. As mentioned earlier, $\left\langle \overline{v_z^{st}{}'(z) v_z^{st}{}'(\xi)} \right\rangle$ is linearly proportional to σ_Y^2. Increasing the heterogeneity causes $\left\langle \overline{v_z{}'(z,t) v_z{}'(\xi,\tau)} \right\rangle$ to increase. What is more interesting, we find that, for a given N_g, the dampening effect of the buoyancy term on velocity fluctuations tends to decrease as σ_Y^2 increases, i.e., $\left\langle \overline{v_z{}'(z,t) v_z{}'(\xi,\tau)} \right\rangle$ is closer to $\left\langle \overline{v_z^{st}{}'(z) v_z^{st}{}'(\xi)} \right\rangle$ in Figure 5*a* than in Figure 4*a*. This behavior is essentially due to the diminished capability of the negative cross-covariances $\left\langle \overline{v_z^{dy}{}'(z,t) v_z^{st}{}'(\xi)} \right\rangle$ and $\left\langle \overline{v_z^{st}{}'(z) v_z^{dy}{}'(\xi,\tau)} \right\rangle$ to stabilize the flow, i.e., the absolute value of $\left\langle \overline{v_z^{dy}{}'(z,t) v_z^{st}{}'(\xi)} \right\rangle$ and $\left\langle \overline{v_z^{st}{}'(z) v_z^{dy}{}'(\xi,\tau)} \right\rangle$ increases sub-linearly with σ_Y^2. To further clarify this aspect, we derive an analytical expression for $\left\langle \overline{v_z^{st}{}'(z) v_z^{dy}{}'(z,t)} \right\rangle$ based on the following set of rough approximations of

(23): (*i*) the buoyancy term is neglected, and (*ii*) $\partial\overline{C}(\xi,\tau)/\partial\xi$ is approximated through a Gaussian function whose degree of spreading for the tracer case is governed by the macro-dispersion coefficient, D^{mt}, (Gelhar and Axness, [25]). Multiplying (23) by $v_z^{st}{}'(z)$ (as in (22)), taking spatial and ensemble expectation and making use of (12) leads to (after some manipulations):

$$\left\langle \overline{v_z^{st}{}'(z)v_z^{dy}{}'(z,t)} \right\rangle \approx \frac{\mathrm{N_g}}{\phi}\int_0^t\int_\Omega \frac{C_Y}{\sqrt{4\pi D^{mt}\tau}}\exp\left(-\frac{(\xi-\tau)^2}{4D^{mt}\tau}\right)G_z^T(z,t;\xi,\tau)d\xi d\tau$$
$$\approx \frac{\mathrm{N_g}}{\phi}\int_0^t\int_\Omega \frac{\sigma_Y}{\sqrt{4\pi l\tau}}\exp\left(-\frac{(\xi-\tau)^2}{l\sigma_Y^2\tau}\right)\exp\left(-\frac{|z-\xi|}{l}\right)G_z^T(z,t;\xi,\tau)d\xi d\tau \qquad (27)$$

which highlights a sublinear grow of the cross-covariance of vertical velocity with σ_Y^2, for a given $\mathrm{N_g}$. Recalling (25) and (26), the sublinear dependence on σ_Y^2 of the cross-covariance between *dynamic* and *stationary* components, when viewed in the context of the linear scaling on σ_Y^2 of the *stationary* velocity covariance, suggests that the effect of stabilization of $\left\langle \overline{v_z^{dy}{}'(z,t)v_z^{st}{}'(\xi)} \right\rangle$ and $\left\langle \overline{v_z^{st}{}'(z)v_z^{dy}{}'(\xi,\tau)} \right\rangle$ on the flow field, and therefore on the solute front, decreases as the heterogeneity of the porous medium increases. We emphasize that the purpose of (27) is not to provide an exact solution of $\left\langle \overline{v_z^{st}{}'(z)v_z^{dy}{}'(\xi,\tau)} \right\rangle$ but to help in clarifying the effects of σ_Y^2 on the *dynamic* and *stationary* velocity cross-covariance.

4.2 Cross Covariance between Concentration and Permeability

Figure 6 depicts the Monte Carlo based section-averaged cross-covariance between permeability and concentration, $\left\langle \overline{Y(z)C'(\xi,\tau)} \right\rangle$, versus ξ when $z = z_2$ (black curves) and versus z when $\xi = \xi_2 = z_2$ (red curves) at time $\tau = t_2 = 4.4\times10^3$ for $\sigma_Y^2 = 0.1$ when $\mathrm{N_g} = 1$ (Figure 6*a*) or 0.1 (Figure 6*b*). Corresponding results for $\sigma_Y^2 = 0.5$ and $\mathrm{N_g} = 1$ or 0.1 are illustrated in Figures 6*c* and 6*d*. Corresponding semi-analytical results are in good agreement (details not shown for clarity). Results

obtained for $\left\langle \overline{Y(z=z_2)C'(\xi,\tau)} \right\rangle$ (blues curves) and $\left\langle \overline{Y(z)C'(\xi=\xi_2,\tau)} \right\rangle$ (green curves) when density is constant are also included.

The analysis of $\left\langle \overline{Y(z)C'(\xi,\tau)} \right\rangle$ versus ξ allows highlighting the way permeability fluctuations, $Y(z)$, are correlated with concentration fluctuation, $C'(\xi,\tau)$, at space-time coordinates (ξ,τ). Otherwise, graphs of $\left\langle \overline{Y(z)C'(\xi,\tau)} \right\rangle$ versus z reveal how concentration fluctuations $C'(\xi,\tau)$ (at a given location) are affected by permeability fluctuations at a set of z spatial coordinates. It can be noted that: (*a*) peaks of $\left\langle \overline{Y(z)C'(\xi,t)} \right\rangle$ do not occur at the selected reference locations ξ_2 or z_2; (*b*) values of $\left\langle \overline{Y(z_2)C'(\xi,t)} \right\rangle$ at $\xi > z_2$ are larger than those at $\xi < z_2$, thus implying that permeability fluctuations influence $C'(\xi,t)$ at downstream (i.e., when $\xi > z_2$) locations along the direction of the mean flow more strongly than they do at $\xi < z_2$. Consistent with this mechanism, $C'(\xi_2,t)$ is highly correlated with $Y(z)$ when $z < \xi_2$ (see red curve in Figure 6). In summary, Figure 6 suggests that (*a*) permeability at a given location highly influences concentration at downstream positions, and (*b*) concentration are highly correlated with permeability at upstream locations. These results also imply that permeability data are expected to be beneficial (on average) to reduce uncertainty on solute transport prediction at downstream (along the mean flow direction) locations, concentration measurements conveying relevant information to infer permeability within upstream zones.

One can note that values of $\left\langle \overline{Y(z)C'(\xi_2,t)} \right\rangle$ for a given z are larger for the constant density than in a variable density scenario (compare green and red curves in Figure 6). The mechanism associated with the reduction of $\left\langle \overline{Y(z)C'(\xi_2,t)} \right\rangle$ for the variable density scenario is elucidated by our semi-analytical solution (E.5). It is linked to the last term on the right hand side of (E.5), which depends linearly on N_g and vanishes in the uniform density case. From a physical point of view, the emerging behavior is due to the capability of the stabilizing buoyant effects of smoothing the perturbation in

the solute concentration profiles induced by the spatial variability of permeability. As a consequence, an increase of buoyancy effects in a heterogeneous domain results in concentration profiles that are characterized by a regular shape, which is akin to the one observed in homogeneous media. Values of $\left\langle \overline{Y(z)C'(\xi,\tau)} \right\rangle$ in density-driven flows tend to coincide with those associated with uniform density scenarios for increasing σ_Y^2 and/or decreasing $\mathrm{N_g}$, because the effect of the stabilizing buoyancy terms decreases.

Comparison of Figures 4 and 6 reveals that the shape of $\left\langle \overline{v_z^{dy}'(z,t)v_z^{st}'(\xi)} \right\rangle$ and $\left\langle \overline{v_z^{st}'(z)v_z^{dy}'(\xi,\tau)} \right\rangle$ is respectively similar to that of $\left\langle \overline{C'(z,t)Y(\xi)} \right\rangle$ and $\left\langle \overline{Y(z)C'(\xi,\tau)} \right\rangle$. This numerical result is in agreement with (D.8)-(D.9), according to which $\left\langle \overline{v_z^{dy}'(z,t)v_z^{st}'(\xi)} \right\rangle \propto -\mathrm{N_g} \left\langle \overline{C'(z,t)Y(\xi)} \right\rangle / \phi$ and $\left\langle \overline{v_z^{st}'(z)v_z^{dy}'(\xi,\tau)} \right\rangle \propto -\mathrm{N_g} \left\langle \overline{Y(z)C'(\xi,\tau)} \right\rangle / \phi$. We remark that our analysis of the cross-covariance between permeability and concentration leads to conclusions which are consistent with those stemming from our discussion about velocity covariances because for the scenario here investigated the characteristics of Y mainly dictate the behavior of v_z^{st}', C' being clearly linked to v_z^{dy}'.

4.3 Ensemble Dispersive Flux and Concentration Variance

Here, we analyze the *ensemble* dispersive flux, $\left\langle \overline{v_z'C'} \right\rangle$ introduced in (24)-(25). We recall (25)-(26) and remark that $\left\langle \overline{v_z'C'} \right\rangle$ depends non-linearly on the mean concentration gradient, $\partial \left\langle \overline{C} \right\rangle / \partial z$. This observation is consistent with previous analytical and numerical results (see, e.g., [31, 32, 60]). The root of this non-linear dependency lies in the coupling between the flow and transport problems and in particular is due to the stabilizing buoyant term in the *dynamic* velocity fluctuations, which depends on the mean concentration gradient, as emphasized by (23).

Figures 7*a* and 7*b* respectively depict $\left\langle \overline{v_z'C'} \right\rangle$ and the concentration variance, $\sigma_c^2 = \left\langle \overline{C'^2} \right\rangle$, versus z at three selected times, for $\sigma_Y^2 = 0.1$ and constant density (blue curves), or $\mathrm{N_g} = 0.1$ (red curves),

and 1 (black curves) computed via Monte Carlo simulations. The semi-analytical solutions of (25), for $\left\langle \overline{v_z'C'} \right\rangle$, and (F.6), for σ_c^2, are also depicted. Corresponding results for $\sigma_Y^2 = 0.5$ are depicted in Figures 7*c* and 7*d*. One can note from Figure 7 that our semi-analytical solutions capture the behavior of the Monte Carlo numerical results. Values of $\left\langle \overline{v_z'C'} \right\rangle$ and σ_c^2 decrease in time and/or for increasing N_g suggesting that $\left\langle \overline{C}(z,t) \right\rangle$ can be considered as a good approximation of (random) concentrations $\overline{C}(z,t)$ and $C(y,z,t)$ (*a*) at late times when the solute front has sampled the overall log-permeability variability and concentration fluctuations along the transverse direction tend to be smoothed out due to mixing, and/or (*b*) for large values of N_g, because the solute front in heterogeneous domains tends to resemble the pattern documented in homogenous media. An increase of the heterogeneity of the permeability field causes both $\left\langle \overline{v_z'C'} \right\rangle$ and σ_c^2 to increase and the regularizing ability of the stabilizing buoyancy effects to decrease for a given N_g. These findings are in agreement with the experimental results of Landman et al. [32]-[33]. Our semi-analytical solutions overestimate the MC based peaks of the dispersive flux and of the concentration variance. This type of behavior has already been detected in second-order analytical and semi-analytical methods developed for constant density scenarios (see, e.g., [28, 41, 42]) and it has been attributed to the observation that such approaches neglect third order moments (involving velocity and concentration fluctuations) that can play a significant role as aquifer heterogeneity, time and Péclet number increase.

The decrease of $\left\langle \overline{v_z'C'} \right\rangle$ and σ_c^2 with N_g is described by our semi-analytical solution (25)-(26) and (F.1) and is linked to the negative cross-covariances, $\left\langle \overline{v_z^{dy}'(z,t)v_z^{st}'(\xi)} \right\rangle$ and $\left\langle \overline{v_z^{st}'(z)v_z^{dy}'(\xi,\tau)} \right\rangle$ analyzed in Section 4.1. Our results embedded in Figures 4 and 5 suggest that the main contribution to the reduction of $\left\langle \overline{v_z'C'} \right\rangle$ and σ_c^2 in a stable variable density setting stems from $\left\langle \overline{v_z^{dy}'(z,t)v_z^{st}'(\xi)} \right\rangle$

. An interpretation of this result can be offered by considering the nature of the problem and noting that the evolution of mean concentration at (z, t) is affected by the perturbations that the velocity field have already experienced, i.e., at times $\tau \le t$ and locations $\xi \le z$. These effects are encapsulated in the Green's function $G_z^T(z,t;\xi,\tau)$ in (25) and (F.1). Note that $\left\langle \overline{v_z^{dy}{}'(z,t)v_z^{st}{}'(\xi)} \right\rangle$ in Figures 4*c*-4*d* and 5*c*-5*d* exhibits long negative tails for $\xi \le z$. The effect of such tails is opposite to the one given by $\left\langle \overline{v_z^{st}{}'(z)v_z^{st}{}'(\xi,\tau)} \right\rangle$. One can see that the convolution between $G_z^T(z,t;\xi,\tau)$ and $\left\langle \overline{v_z^{dy}{}'(z,t)v_z^{st}{}'(\xi)} \right\rangle$ in (25) yields a net reduction of the memory of concentration perturbation on the experienced velocity field due to the stabilizing effects of the density-driven scenario.

5 Conclusions

We analyze the reduction of solute spreading in randomly heterogeneous porous media driven by density variations in a stable flow setting. A key finding of this study is that the reduction of spreading and contraction of concentration profiles are due to a spatial reorganization of the velocity field, as compared to a constant density scenario. We observe that the velocity variance and the spatial extent of velocity correlation tend to decrease when density effects are considered. This reduction of variance and correlation scale of velocity causes a corresponding reduction of the strength of the dispersive flux.

We quantify the reduction of the velocity fluctuations variance and of solute spreading/dispersion for density-driven flows by decomposing the flow field fluctuations into a *stationary* component, $v_z^{st}{}'$, associated with the solution of the flow problem for a constant density fluid, and a *dynamic* component, $v_z^{dy}{}'$, which takes into account the coupling between transport and flow phenomena introduced by density variations. This decomposition enables us to highlight the interplay between permeability, velocity, and concentration, which is what triggers the reduction of spreading we observe when comparing constant and variable density settings.

The origin of the solute dispersion reduction is linked, both from a mathematical and a physical point of view, to the emergence of negative cross-covariances between stationary and dynamic velocity fluctuations, $\left\langle \overline{v_z^{dy}{}' v_z^{st}{}'} \right\rangle$. These cross-covariances describe the interplay between permeability-induced *stationary* fluctuations (which promote solute spreading) and stabilizing buoyancy-induced *dynamic* fluctuations (which hinder solute spreading). We analyze the way these cross-covariances vary with the intensity of the ratio between buoyancy and viscous forces (as expressed by N_g) and with the heterogeneity of the permeability field (as quantified by σ_Y^2). The absolute values of $\left\langle \overline{v_z^{dy}{}' v_z^{st}{}'} \right\rangle$ scale approximately linearly with N_g (i.e., with permeability and density contrast) and sub-linearly with σ_Y^2. This is in contrast with the well-known linear scaling in σ_Y^2 exhibited by the stationary (i.e., constant density) cross-covariance, $\left\langle \overline{v_z^{st}{}' v_z^{st}{}'} \right\rangle$. Therefore, the relative importance of the stabilizing components induced by density variations tends to decrease as the heterogeneity of the porous medium increases. The reduction of the strength of the dispersive flux as well as of the concentration variance which is observed for stable density-driven flow (in comparison with the constant density setting) tends to be stronger for increasing values of N_g and decreasing values of σ_Y^2.

Our study allows investigating the factors controlling the dispersive flux, which is typically interpreted as an upscaled parameter to be estimated through model calibration in field scale density driven problems. A key result of our study is that such a parameter does not depend solely on the aquifer properties (such as permeability) but also on flow and transport variables (such as velocity and solute concentration). As such, dispersion coefficients used in a variable density flow and transport models should vary not only in space but also in time to properly represent flow and transport processes. Investigation of processes underpinning the spreading in unstable density-driven flows as well as applications of the developed approaches to estimate the upscaled dispersive flux in field scale scenarios are envisioned to be the focus of future studies.

Acknowledgment

Funding from MIUR (Italian ministry of Education, University and Research, Water JPI, WaterWorks 2014, Project: WE-NEED- Water NEEDs, availability, quality and sustainability) and CICYT (Project MEDISTRAES) is acknowledged.

References

[1] Abarca E, Carrera J, Sanchez-Vila X, Dentz M. Anisotropic dispersive Henry problem. Adv Water Resour 2007; 30(4):913–26. doi: 10.1016/j.advwatres.2006.08.005.

[2] Alkindi A, Al-Wahaibi Y, Bijelic B, Muggeridge A. Investigation of longitudinal and transverse dispersion in stable displacements with high viscosity and density contrast between the fluids. J Contam. Hydrol 2011;120-121:170-183. doi:10.1016/j.jconhyd.2010.06.006.

[3] Bianchi Janetti E, Riva M, Guadagnini A. Three-Phase Permeabilities: Upscaling, Analytical Solutions and Uncertainty Analysis in Elementary Pore Structures. Transp Porous Med 2015;106:259–283. doi 10.1007/s11242-014-0400-x.

[4] Bianchi Janetti E., M. Riva, A. Guadagnini. Effects of Pore-Scale Geometry and Wettability on Two-Phase Relative Permeabilities within Elementary Cells, Water, 9, 252, 2017 doi: 10.3390/w9040252.

[5] Bolster D, Neuwlier I, Dentz M, Carrera J. The impact of buoyancy on front spreading in heterogenous porous media in two-phase immiscible flow. Water Resour Res 2011;47:W02508. doi:10.1029/2010WR009399.

[6] Bolster D, Dentz M, Carrera J. Effective two phase flow in heterogeneous media under temporal pressure fluctuations. Water Resour Res 2009;45:W05408. doi:10.1029/2008WR007460.

[7] Boso F., de Barros F P J, Fiori A, Bellin A. Performance analysis of statistical spatial measures for contaminant plume characterization toward risk-based decision making. Water Resour Res 2013;49:3119–3132. doi:10.1002/wrcr.20270.

[8] Bouquain J, Meheust Y, Davy P. Horizontal pre-asymptotic solute transport in a plane fracture with significant density contrasts. J Contam Hydrol 2011;120-121:184-197. doi:10.1016/j.jconhyd.2010.08.002.

[9] Buès M A, Aachib M. Influence of the heterogeneity of the solutions on the parameters of miscible displacement in saturated porous medium. Exp Fluids 1991;11(1):25-32.

[10] Butkovskiy A G. Green's function and transfer function handbook. Halstead Press, New York, 1982.

[11] Ciriello V, Guadagnini A, Di Federico V, Edery Y, Berkowitz B. Comparative analysis of formulations for conservative transport in porous media through sensitivity-based parameters calibration. Water Resour Res 2013;49:5206-5220. doi: 10.1002/wrcr.20395.

[12] Cushman J H, Bennethum L S, Hu B X. A primer on upscaling tools for porous media. Adv Water Res 2002;25:1043–1067.

[13] D'Angelo M V, Auradou H, Allain C, Rosen M, Hulin J P. Dispersion enhancement and damping by buoyancy driven flows in two-dimensional networks of capillaries. Phys Fluids 2008;20,034107. doi: 10.1063/1.2899635.

[14] Dagan G. Solute transport in heterogeneous porous formations. J Fluid Mech 1984;145:151–177.

[15] Davit Y, Bell C G, Byrne H M, Chapman L A C, Kimpton L S, Lang G E, Leonard K H L, Oliver J M, Pearson N C, Shipley R J, Waters S L, Whiteley J P, Wood B D, Quintard M. Homogenization via formal multiscale asymptotics and volume averaging: how do the two techniques compare?. Adv Water Resour 2013;62:178-206. doi: 10.1016/j.advwatres.2013.09.006.

[16] de Barros F P J, Dentz M. Pictures of blockscale transport: Effective versus ensemble dispersion and its uncertainty. Adv Water Resour 2015;91:11-22. doi:10.1016/j.advwaters.2016.03.004.

[17] Dentz M, Carrera J. Effective solute transport in temporally fluctuating flow through heterogeneous media. Water Resour Res 2005;41:W08414. doi:10.1029/2004WR003571.

[18] Dentz M, Tartakovsky D M, Abarca E, Guadagnini A, Sanchez-Vila X, Carrera J. Variable-density flow in porous media. J Fluid Mech 2006;561:209-35. doi: 10.1017/S0022112006000668.

[19] Dentz M, Tartakovsky D M. Abrupt-Interface Solution for Carbon Dioxide Injection into Porous Media. Transp. Porous Med 2009;79:15-27. doi 10.1007/s11242-008-9268-y.

[20] Deutsch C V, Journel A G. GSLIB: Geostatisitcal Software Library and User's Guide, 2nd Ed. New York. Oxford Univerity Press. 1998.

[21] Di Donato G, Lu H, Tavassoli Z, Blunt M J. Multirate-Transfer dual porosity modelling of gravity drainage and imbibition. SPE Journal 2007;12(01):77-88. doi: 10.2118/93144-PA.

[22] Diersch H J, Kolditz O. Variable-density flow and transport in porous media: approaches and challenges. Adv Water Resour 2002;25(8-12):899-944. doi:10.1016/S0309-1708(02)00063-5.

[23] Edery Y, Guadagnini A, Scher H, Berkowitz B. Origins of anomalous transport in heterogenous media: Structural and dynamic controls. Water Resour Res 2014;50:1490-1505. doi:10.1002/2013WR015111.

[24] Flowers T C, Hunt J R. Viscous and gravitational contributions to mixing during vertical brine transport in water-saturated porous media. Water Resour Res 2007;43:W01407. doi:10.1029/2005WR004773.

[25] Gelhar L W, Axness C L. Three-dimensional stochastic analysis of macrodispersion in aquifers. Water Resour Res 1983;19(1):161–180.

[26] Gramling C M, Harvey C F, Meigs L C. Reactive transport in porous media: A comparison of model prediction with laboratory visualization. Environ Sci Technol 2002;36:2508–2514. doi:10.1021/es0157144.

[27] Hagoort J. Oil recovery by gravity drainage. SPE Journal 1980;20(03):139-150. doi: 10.2118/7424-PA.

[28] Hassanizadeh S M, Leijnse A. A non-linear theory of high-concentration-gradient dispersion in porous media. Adv Water Resour 1995;18(4):203-15. doi:10.1016/0309-1708(95)00012-8.

[29] Held R, Attinger S, Kinzelbach W. Homogenization and effective parameters for the Henry problem in heterogeneous formations. Water Resour Res 2005;41:1-14. doi: 10.1029/2004WR003674.

[30] Jiao C Y, Hötzl H. An experimental study of miscible displacements in porous media with variation of fluid density and viscosity. Transp Porous Med 2004;54:125-44. doi:10.1023/A:1026383019300.

[31] Landman A J, Johannsen K, Schotting R J. Density-dependent dispersion in heterogeneous porous media. Part I: A numerical study. Adv Water Resour 2007a;30(12):2467-2480. doi:10.1016/j.advwatres.2007.05.016.

[32] Landman A J, Schotting R J, Egorov A, Demidov D. Density-dependent dispersion in heterogeneous porous media Part II: Comparison with nonlinear models. Adv Water Resour 2007b;30(12):2481-2498. doi:10.1016/j.advwatres.2007.05.017.

[33] Leij F J, Van Genuchten M T. Analytical modeling of nonaqueous phase liquid dissolution with Green's function. Transp Porous Med 2000;38:141-166. doi:10.1023/A:1006611200487.

[34] Loggia D, Rakotomalala N, Salin D, Yortsos Y C. Phase diagram of miscible displacements in layered porous media. Europhys Lett 1996;36:105-110. doi:10.1029/2001WR001244.

[35] Kempers L J T M, Haas H. The dispersion zone between fluids with different density and viscosity in a heterogeneous porous medium. J Fluid Mech 1994;267:299–324. doi: 10.1017/S0022112094001199.

[36] Kerrou J, Renard P. A numerical analysis of dimensionality and heterogeneity effects on advective dispersive seawater intrusion processes. Hydrol. J. 2010;18:55-72. doi: 10.1007/s10040-009-0533-0.

[37] Kretz V, Berest P, Hulin J P, Salin D. An experimental study of the effects of density and viscosity contrasts on macrodispersion in porous media. Water Resour Res 2003;39(2):1032-1040. doi:10.1029/2001WR001244.

[38] Konz M, Younes A, Ackerer P, Fahs M, Huggenberger P, Zechner E. Variable-density flow in heterogeneous porous media - Laboratory experiments and numerical simulations. J Contam Hydrol 2009;108(3-4):168-175. doi: 10.1016/j.jconhyd.2009.07.005.

[39] Menand T, Woods A W. Dispersion, scale, and time dependence of mixing zones under gravitationally stable and unstable displacements in porous media. Water Resour Res 2005;41:W05014. doi: 10.1029/2004WR003701.

[40] Monger T G, Ramos J C, Thomas J. Light oil recovery from cyclic CO2 injection: influence of low pressure, impure CO2 and reservoir gas. SPE Reservoir Engineering 1991;6:25-32. doi: 10.2118/18084-PA.

[41] Morales-Casique E, Neuman S P, Guadagnini A. Non-local and localized analyses of non-reactive solute transport in bounded randomly heterogeneous porous media: Theoretical framework. Adv Water Resour 2006a;29:1238-1255.

[42] Morales-Casique E, Neuman S P, Guadagnini A. Non-local and localized analyses of non-reactive solute transport in bounded randomly heterogeneous porous media: Computational analysis. Adv Water Resour 2006b;29:1399-1418.

[43] Naff R L. On the nature of the dispersive flux in saturated heterogeneous porous media. Water Resour Res 1990;26(5):1013-1026.

[44] Neuman S P, Tartakovsky D M. Perspective on theories of non-Fickian transport in heterogeneous media. Adv Water Resour 2009;32(5):670-680.

[45] Nick H M, Schotting R, Gutierrez-Neri M, Johannsen K. Modelling transverse dispersion and variable density flow in porous media. Transp Porous Med 2009;78:11-35. doi:10.1007/s11242-008-9277-x.

[46] Oostrom M, Dane J H, Güven O, Hayworth J S. Experimental investigation of dense solute plumes in an unconfined aquifer model. Water Resour Res 1992a;28(9):2315-2326. doi:10.1029/92WR01265.

[47] Oostrom M, Hayworth J S, Dane J H, Güven O. Behavior of dense aqueous leachate plumes in homogeneous porous media. Water Resour Res 1192b;28(8):2123-2134. doi:10.1029/92WR00711.

[48] Pool M, Carrera J, Vilarrasa V, Silva O, Ayora C. Dynamics and design of systems for geological storage of dissolved CO2. Adv Water Resour 2013;62:533-542.

[49] Porta G M, Bijeljic B, Blunt M J, Guadagnini A. Continuum-scale characterization of solute transport based on pore-scale velocity distributions. Geophy Res Lett 2015;42(18):7537-7545. doi:10.1002/2015GL065423.

[50] Rhodes M E, Bijeljic B, Blunt M J. A rigorous pore-to-field scale simulation methodology for single-phase flow based on continuous time random walk. SPE Journal 2009;14(1):88-94. doi: 10.2118/106434-MS.

[51] Riva M, Guadagnini A, Dell'Oca A. Probabilistic assessment of seawater intrusion under multiple sources of uncertainty, Adv. Water Res, 75, 93-104, doi:10.1016/j.advwatres.2014.11.002

[52] Sanchez-Vila X, Fernàndez-Garcia D, Guadagnini A. Interpretation of column experiments of transport of solutes undergoing an irreversible bimolecular reaction using a continuum approximation. Water Resour Res 2010;46:W12510. doi:10.1029/2010WR009539.

[53] Sebben M L, Werner A D, Graf T. Seawater intrusion in fractured aquifers: A preliminary numerical investigation using a fractured Henry problem. Adv Water Resour 2015;85:93-108. doi:10.1016/j.advwatres.2015.09.013.

[54] Siena M, Guadagnini A, Riva M, Bijelijic B, Perreira Nunes J P, Blunt M J. Statistical scaling of pore-scale Lagrangian velocities in natural porous media. Phys. Rev. E 2014;90:023013. doi:10.1103/PhysRevE.90.023013.

[55] Simmons C T, Fenstemaker T R, Sharp J M. Variable density groundwater flow and solute transport in heterogeneous porous media: Approaches, resolutions and future challenges. J Contam Hydrol 2001;52(1-4):245-275. doi:10.1016/S0169-7722(01)00160-7.

[56] Sun T, Mehmani Y, Bhagmane J, Balhoff M T. Pore to continuum upscaling of permeability in heterogeneous porous media using mortars. Int J Oil, Gas and Coal Technology 2012; 5(2-3).

[57] Tenchine S, Gouze P. Density contrast effects on tracer dispersion in variable aperture fractures. Adv Water Resour 2005;28:273-289. doi: 10.1016/j.advwatres.2004.10.009.

[58] Voss C I, Provost A M. SUTRA, a model for saturate–unsaturated variable density ground-water with solute or energy transport. U S Geol Surv Water Resour Invest Rep 2002;02-4231.

[59] Watson S J, Barry D A, Schotting R J, Hassanizadeh S M. Validation of classical density-dependent solute transport theory for stable, high concentration-gradient brine displacements in coarse and medium sands. Adv Water Resour 2002;25:611-35. doi:10.1016/S0309-1708(02)00022-2.

[60] Welty C, Gelhar L W. Stochastic analysis of the effect of fluid density and viscosity variability on macrodispersion in heterogeneous porous media. Water Resour Res 1991;27(8):2061–75. doi:10.1029/91WR00837.

[61] Welty C, Kane III A C, Kaufman L J. Stochastic analysis of transverse dispersion in density-coupled transport in aquifers. Water Resour Res 2003;39(6):1150. doi:10.1029/2002WR001631.

[62] Werner A D, Bakker M, Post V E A, Vandenbohede A, Lu C, Ataie-Ashtiani B, Simmons C T, Barry D A. Seawater intrusion processes, investigation and management: recent advances and future challenges. Adv Water Resour 2013;51:3-26. doi: 10.1016/j.advwatres.2012.03.004.

[63] Whitaker S. The Method of Volume Averaging. Kluwer, Dordrecht 1999.

[64] Woumeni R S, Vauclin M. A field study of the coupled effects of aquifer stratification, fluid density, and groundwater fluctuations on dispersivity assessment. Adv Water Resour 2006; 29(7):1037-1055. doi:10.1016/j.advwatres.2005.09.002.

[65] Xu X, Chen S, Zhang D. Convective stability analysis of the long-term storage of carbon dioxide in deep saline aquifers. Adv Water Resour 2005;29(3):397-407. doi:10.1016/j.advwatres.2005.05.008.

[66] Zoia A, Latrille C, Beccantini A, Cartadale A. Spatial and temporal features of density-dependent contaminant transport: experimental investigation and numerical modelling. J Contam Hydrol 2009;109(1-4):14-26. doi: 10.1016/j.jconhyd.2009.07.006.

Appendix A. Section averaged concentration and effective dispersive flux

Substituting (16)-(17) in (15), applying the spatial mean operator (13) and making use of the first of (14), leads to the following equation

$$\frac{\partial \overline{C}}{\partial t}+\overline{v}_z\frac{\partial \overline{C}}{\partial z}-\frac{\partial}{\partial z}\left(\overline{D_{zz}}\frac{\partial \overline{C}}{\partial z}\right)+\frac{\partial \overline{v_z'C'}}{\partial z}-\frac{\partial}{\partial z}\left(\overline{D_{zz}'\frac{\partial C'}{\partial z}}\right)=0\,, \tag{A.1}$$

satisfied by the spatially-averaged concentration, $\overline{C}(z,t)$, for the problem set up depicted in Figure 1. Here,

$$\overline{D_{zz}}=\frac{1}{W}\int_0^W D_{zz}(y,z,t)dy=\frac{1}{WPe}\int_0^W\left|\boldsymbol{v}(y,z,t)\right|dy=\frac{\left|\overline{\boldsymbol{v}}(z,t)\right|}{Pe}\approx\frac{\overline{v_z}}{Pe},$$
$$\overline{v_z'C'}=\frac{1}{W}\int_0^W v_z'(y,z,t)C'(y,z,t)dy,\qquad \overline{D_{zz}'\frac{\partial C'}{\partial z}}=\frac{1}{W}\int_0^W D_{zz}'(y,z,t)\frac{\partial}{\partial z}C'(y,z,t)dy. \tag{A.2}$$

Applying (13) to the first of (14) and considering decomposition (16) yields

$$\nabla\cdot\left(\overline{\boldsymbol{v}(z,t)+\boldsymbol{v}'(z,t)}\right)=\frac{\partial\overline{v}_z(z,t)}{\partial z}=0\,,\qquad \overline{v}_z(z,t)=v_{BC}=1 \tag{A.3}$$

i.e., the spatial mean of the vertical velocity is constant and coincides with the prescribed vertical velocity at $z = H$. A numerical analysis allows recognizing that it is possible to neglect the last term of (A.1) (details not shown). Moreover, making use of (A.2) and (A.3), $\overline{D_{zz}}$ can be approximated as 1/Pe. This leads to

$$\frac{\partial \overline{C}}{\partial t}+\frac{\partial \overline{C}}{\partial z}-\frac{1}{\mathrm{Pe}}\frac{\partial^2\overline{C}}{\partial z^2}+\frac{\partial \overline{v_z'C'}}{\partial z}=0\,, \tag{A.4}$$

where $\overline{v_z'C'}$ is the *single realization* dispersive flux discussed in Section 3.1. Closure of (A.4) is obtained upon writing $\overline{v_z'C'}$ as a function of $\overline{C}$, as detailed in the following. Subtracting (A.4) from (15) and neglecting terms involving the product of fluctuations yields

$$\frac{\partial C'}{\partial t}+\frac{\partial}{\partial z}C'-\frac{\nabla^2C'}{\mathrm{Pe}}=-\boldsymbol{v}'\cdot\nabla\overline{C}+\nabla\cdot\left(\boldsymbol{D}'\nabla\overline{C}(z,t)\right). \tag{A.5}$$

Numerical simulations show that $-\boldsymbol{v}'\cdot\nabla\overline{C}>>\nabla\cdot\left(\boldsymbol{D}'\nabla\overline{C}\right)$ (details not shown) so that (A.5) simplifies as

$$\frac{\partial C'}{\partial t}+\frac{\partial}{\partial z}C'-\frac{\nabla^2C'}{\mathrm{Pe}}=-v_z'\frac{\partial}{\partial z}\overline{C}\,, \tag{A.6}$$

subject to the following (homogeneous) boundary and initial conditions

$$C'(y,z=0,t)=0, \qquad C'(y,z=H,t)-\frac{1}{\mathrm{Pe}}\frac{\partial C'(y,z,t)}{\partial z}=0,$$
$$\frac{\partial C'(y=0,z,t)}{\partial y}=\frac{\partial C'(y=W,z,t)}{\partial y}=0, \qquad C'(y,z,t=0)=0. \tag{A.7}$$

Solution of (A.6) can be expressed in terms of G^T, i.e., the Green's function that satisfies (A.6)-(A.7) with the source term replaced by $\delta(\eta-y)\delta(\xi-z)\delta(t-\tau)$, where δ is the Dirac' delta function, as

$$C'(y,z,t)=-\int_0^t\int_\Omega v_z'(\eta,\xi,\tau)\frac{\partial}{\partial\xi}\overline{C}(\xi,\tau)G^T(y,z,t;\xi,\eta,\tau)d\eta d\xi d\tau. \tag{A.8}$$

Multiplying (A.8) by $v_z'(y,z,t)$ and applying (13) leads to the following expression for the *single realization* dispersive flux

$$\overline{v_z'(z,t)C'(z,t)}=-\int_0^t\int_\Omega \overline{v_z'(z,t)G^T(z,t;\eta,\xi,\tau)}\,v_z'(\eta,\xi,\tau)\frac{\partial\overline{C}(\xi,\tau)}{\partial\xi}d\eta d\xi d\tau, \tag{A.9a}$$

with

$$\overline{v_z'(z,t)G^T(z,t;\eta,\xi,\tau)}=\frac{1}{W}\int_0^W v_z'(y,z,t)G^T(y,z,t;\eta,\xi,\tau)dy. \tag{A.9b}$$

We further simplify our analysis and follow Bolster et al. [5], [6] by considering a one-dimensional (1D) problem (along the vertical *z*-direction) within a semi-infinite domain, $z\in[0,\infty)$. Under this setting, a closed-form analytical expression for G^T is (see [33])

$$G^T(y,z,t;\xi,\eta,\tau)=\delta(y-\eta)G_z^T(z,t;\xi,\tau)$$
$$\text{with}\quad G_z^T(z,t;\xi,\tau)=\sqrt{\frac{\mathrm{Pe}}{4\pi(t-\tau)}}\left[e^{-\mathrm{Pe}\left(\frac{(z-\xi-t+\tau)^2}{4(t-\tau)}\right)}-e^{\mathrm{Pe}\left(z-\frac{(\xi+z+t-\tau))^2}{4(t-\tau)}\right)}\right]. \tag{A.10}$$

Making use of (A.10), (A.9a) simplifies as

$$\overline{v_z'(z,t)C'(z,t)}=-\int_0^t\int_0^H \overline{v_z'(z,t)v_z'(\xi,\tau)}\,G_z^T(z,t,\xi,\tau)\frac{\partial\overline{C}(\xi,\tau)}{\partial\xi}d\xi d\tau, \tag{A.11a}$$

with

$$\overline{v_z'(z,t)v_z'(\xi,\tau)} = \frac{1}{W}\int_0^W v_z'(y,z,t)v_z'(y,\xi,\tau)dy\,. \tag{A.11b}$$

Note that $\eta = y$ by virtue of (A.10), so that only the product of velocity fluctuations along the same vertical locations is retained in (A.11a) and (A.11.b).

Appendix B. Ensemble mean of section-averaged concentration and ensemble dispersive flux

Applying the ensemble mean operator to (A.4) yields

$$\frac{\partial\langle\bar{C}\rangle}{\partial t} + \frac{\partial\langle\bar{C}\rangle}{\partial z} - \frac{1}{\mathrm{Pe}}\frac{\partial^2\langle\bar{C}\rangle}{\partial z^2} = -\frac{\partial\langle\overline{v_z'C'}\rangle}{\partial z} \tag{B.1}$$

where $\langle\overline{v_z'C'}\rangle$ is the ensemble dispersive flux discussed in Section 3.2. This term can be evaluated applying the ensemble averaging operator to (A.11a) and neglecting terms involving products of fluctuations of order higher than two, as

$$\langle\overline{v_z'(z,t)C'(z,t)}\rangle = -\int_0^t\int_0^H \langle\overline{v_z'(z,t)v_z'(\xi,\tau)}\rangle \frac{\partial\langle\bar{C}(\xi,\tau)\rangle}{\partial\xi} G_z^T(z,t,\xi,\tau)d\xi d\tau\,. \tag{B.2}$$

Equation (B.2) clearly elucidates that the ensemble dispersive flux is a non-local quantity in time and space, as it depends on velocity cross-covariances and concentration gradients evaluated across the whole domain at all times $\tau \le t$. A (partial) localization of (B.2) is offered by

$$\langle\overline{v_z'(z,t)C'(z,t)}\rangle = -\int_0^t\int_0^H \langle\overline{v_z'(z,t)v_z'(\xi,\tau)}\rangle G_z^T(z,t,\xi,\tau)d\xi d\tau \frac{\partial\langle\bar{C}(z,t)\rangle}{\partial z} \tag{B.3}$$

Appendix C. Velocity and pressure Fluctuations

A first order approximation of velocity fluctuation components $v_y'(y,z,t)$ and $v_z'(y,z,t)$ defined in (16) are derived by subtracting the spatial mean of velocity from the second of (14), approximating the permeability fluctuation as $k'(y,z) = \exp(Y(y,z)) - 1 \approx Y(y,z)$ and disregarding terms involving the product of fluctuations, as

$$v_y'(y,z,t) = -\frac{1}{\phi}\frac{\partial p'(y,z,t)}{\partial y} \tag{C.1}$$

$$v_z'(y,z,t) = Y(y,z) - \frac{1}{\phi}\left(\frac{\partial p'(y,z,t)}{\partial z} + \mathrm{N_g}\,\rho'(y,z,t)\right). \tag{C.2}$$

Note that (20) and (A.3) enable us to write

$$\bar{v}_z(z,t) = 1 = \bar{v}_z^{st}(z) + \bar{v}_z^{dy}(z,t) = \bar{v}_z^{st}, \qquad \bar{v}_z^{dy}(z,t) = 0\,. \tag{C.3}$$

Recalling the *stationary* and *dynamic* decomposition introduced in (20) and (C.3) allows rewriting (C.1)-(C.2) as

$$v_y^{st}{}'(y,z) = -\frac{1}{\phi}\frac{\partial p^{st}{}'(y,z)}{\partial y}, \qquad v_y^{dy}{}'(y,z,t) = -\frac{1}{\phi}\frac{\partial p^{dy}{}'(y,z,t)}{\partial y}, \tag{C.4}$$

$$v_z^{st}{}'(y,z) = Y(y,z) - \frac{1}{\phi}\frac{\partial p^{st}{}'(y,z)}{\partial z}, \qquad v_z^{dy}{}'(y,z,t) = -\frac{1}{\phi}\left(\frac{\partial p^{dy}{}'(y,z,t)}{\partial z} + \mathrm{N_g}\,\rho'(y,z,t)\right), \tag{C.5}$$

where $p^{st}{}'(y,z)$ and $p^{dy}{}'(y,z,t)$ respectively are *stationary* and *dynamic* pressure fluctuations. Using (C.4) and (C.5) and noting that $\boldsymbol{v}^{st}$ is divergence-free yields

$$\nabla^2 p^{st}{}'(y,z) = \phi\frac{\partial Y(y,z)}{\partial z}. \tag{C.6}$$

Note that (C.6) coincides with the first order approximation of the equation of constant density flow through heterogeneous media. Considering the set-up of Figure 1, equation (C.6) is subject to the following boundary conditions

$$p^{st}{}'(y,z=0) = 0, \quad \frac{\partial p^{st}{}'(y,z=H)}{\partial z} = 0, \quad \frac{\partial p^{st}{}'(y=0,z)}{\partial y} = \frac{\partial p^{st}{}'(y=W,z)}{\partial y} = 0. \tag{C.7}$$

Solution of (C.6)-(C.7) is

$$p^{st}{}'(y,z) = \phi\int_{\Omega}\frac{\partial}{\partial\xi}Y(\eta,\xi)\,G^{F}(y,z;\eta,\xi)\,d\eta d\xi \tag{C.8}$$

where $G^{F}(y,z;\eta,\xi)$ is a Green's function, i.e., it satisfies (C.6)-(C.7) with the source term replaced by $\delta(\eta-y)\delta(\xi-z)$.

A similar procedure yields the following equation satisfied by pressure perturbations

$$\nabla^2 p'(y,z,t) = \phi\frac{\partial Y(y,z)}{\partial z} - \mathrm{N_g}\frac{\partial\rho'(y,z,t)}{\partial z}. \tag{C.9}$$

Subtracting (C.6) from (C.9) and making use of (17) yields the following equation satisfied by the dynamic pressure fluctuation

$$\nabla^2 p^{dy}{}'(y,z,t) = -\mathrm{N_g}\frac{\partial C'(y,z,t)}{\partial z}, \tag{C.10}$$

subject to the boundary and initial conditions

$$p^{dy}{}'(y,z=0,t) = 0, \quad \frac{\partial p^{dy}{}'(y,z=H,t)}{\partial z} = 0, \quad \frac{\partial p^{dy}{}'(y=0,z,t)}{\partial y} = \frac{\partial p^{dy}{}'(y=W,z,t)}{\partial y} = 0,$$
$$p^{dy}{}'(y,z,t=0) = 0. \tag{C.11}$$

Solution of (C.10)-(C.11) is given by

$$p^{dy}{}'(y,z,t) = -\mathrm{N_g}\int_{\Omega}\frac{\partial C'(\eta,\xi,t)}{\partial\xi}G^{F}(y,z;\eta,\xi)d\eta d\xi\,. \tag{C.12}$$

Appendix D. Covariance of Vertical Velocity

Making use of (20), the horizontal spatial mean of the covariance of vertical velocity components can be written as

$$\left\langle\overline{v'_z(z,t)v'_z(\xi,\tau)}\right\rangle = \left\langle\overline{v_z^{st}{}'(z)v_z^{st}{}'(\xi)}\right\rangle+\left\langle\overline{v_z^{st}{}'(z)v_z^{dy}{}'(\xi,\tau)}\right\rangle+\left\langle\overline{v_z^{dy}{}'(z,t)v_z^{st}{}'(\xi)}\right\rangle+\left\langle\overline{v_z^{dy}{}'(z,t)v_z^{dy}{}'(\xi,\tau)}\right\rangle \tag{D.1}$$

Considering (C.5) and (17), enables us to write $\left\langle\overline{v_z^{st}{}'(z)v_z^{dy}{}'(\xi,\tau)}\right\rangle$ as

$$\begin{aligned}\left\langle\overline{v_z^{st}{}'(z)v_z^{dy}{}'(\xi,\tau)}\right\rangle = &-\frac{1}{\phi}\left[\frac{\partial}{\partial\xi}\left\langle\overline{Y(z)p^{dy}{}'(\xi,\tau)}\right\rangle-\frac{1}{\phi}\frac{\partial^2}{\partial z\partial\xi}\left\langle\overline{p^{st}{}'(z)p^{dy}{}'(\xi,\tau)}\right\rangle\right]\\ &-\frac{\mathrm{N_g}}{\phi}\left[\left\langle\overline{Y(z)C'(\xi,\tau)}\right\rangle-\frac{1}{\phi}\left\langle\overline{\frac{\partial p^{st}{}'(z)}{\partial z}C'(\xi,\tau)}\right\rangle\right].\end{aligned} \tag{D.2}$$

Recalling (C.12), the first term on right hand side of (D.2) can be computed as

$$\begin{aligned}-\frac{1}{\phi}\frac{\partial}{\partial\xi}\left\langle\overline{Y(z)p^{dy}{}'(\xi,\tau)}\right\rangle &= -\frac{1}{\phi W}\int_0^W\frac{\partial}{\partial\xi}\left\langle Y(z,y)p^{dy}{}'(\xi,y,\tau)\right\rangle dy\\ &= \frac{\mathrm{N_g}}{\phi W}\int_0^W\int_0^H\int_0^W\frac{\partial}{\partial\hat{\xi}}\left\langle Y(z,y)C'(\hat{\eta},\hat{\xi},\tau)\right\rangle\frac{\partial}{\partial\xi}G^{F}(y,\xi;\hat{\eta},\hat{\xi})d\hat{\eta}d\hat{\xi}dy\end{aligned}\,. \tag{D.3}$$

We then approximate $G^{F}(y,\xi;\hat{\eta},\hat{\xi})$ as

$$G^{F}(y,\xi;\hat{\eta},\hat{\xi}) = \delta\left(y-\hat{\eta}\right)G^{F}(\xi;\hat{\xi}), \tag{D.4a}$$

with [10]

$$G^{F}(\xi;\hat{\xi}) = \begin{cases}\ln\dfrac{H}{H-\xi}-2\displaystyle\sum_{n=1}^{\infty}I_0\left(\lambda_n,\hat{\xi}\right)\left[\dfrac{K_0\left(\lambda_n,H\right)}{I_0\left(\lambda_n,H\right)}I_0\left(\lambda_n,H-\xi\right)-K_0\left(\lambda_n,H-\xi\right)\right] & \text{if}\quad 0\le\xi\le H-\hat{\xi}\\ \ln\dfrac{H}{\hat{\xi}}-2\displaystyle\sum_{n=1}^{\infty}I_0\left(\lambda_n,H-\xi\right)\left[\dfrac{K_0\left(\lambda_n,H\right)}{I_0\left(\lambda_n,H\right)}I_0\left(\lambda_n,\hat{\xi}\right)-K_0\left(\lambda_n,\hat{\xi}\right)\right] & \text{if}\quad H-\hat{\xi}\le\xi\le H\end{cases} \tag{D.4b}$$

Here, I_0 and K_0 respectively are the modified Bessel function of first and second kind and $\lambda_n = n\pi/H$. Making use of (D.4a), (D.3) becomes

$$-\frac{1}{\phi}\frac{\partial}{\partial\xi}\left\langle\overline{Y(z)p^{dy}{}'(\xi,\tau)}\right\rangle\approx\frac{\mathrm{N_g}}{\phi W}\int_0^H\int_0^W\frac{\partial}{\partial\hat{\xi}}\left\langle Y(z,y)C'(\hat{\eta}=y,\hat{\xi},\tau)\right\rangle\frac{\partial}{\partial\xi}G^F(\xi;\hat{\xi})dyd\hat{\xi}$$
$$=\frac{\mathrm{N_g}}{\phi}\int_0^H\frac{\partial}{\partial\hat{\xi}}\left\langle\overline{Y(z)C'(\hat{\xi},\tau)}\right\rangle\frac{\partial}{\partial\xi}G^F(\xi;\hat{\xi})d\hat{\xi}. \tag{D.5}$$

A similar procedure yields the following expressions for the remaining terms of (D.2)

$$\frac{1}{\phi^2}\frac{\partial^2}{\partial z\partial\xi}\left\langle\overline{p^{st}{}'(z)p^{dy}{}'(\xi,\tau)}\right\rangle\approx-\frac{\mathrm{N_g}}{\phi}\int_0^H\int_0^H\frac{\partial^2}{\partial\tilde{\xi}\partial\xi}\left\langle\overline{Y(\tilde{\xi})C'(\xi,\tau)}\right\rangle\frac{\partial}{\partial\xi}G^F(\xi;\hat{\xi})\frac{\partial}{\partial z}G^F(z;\tilde{\xi})d\xi d\tilde{\xi} \tag{D.6}$$

$$\frac{\mathrm{N_g}}{\phi^2}\frac{\partial}{\partial z}\left\langle\overline{p^{st}{}'(z)C'(\xi,\tau)}\right\rangle\approx\frac{\mathrm{N_g}}{\phi}\int_0^H\frac{\partial}{\partial\tilde{\xi}}\left\langle\overline{Y(\tilde{\xi})C'(\xi,\tau)}\right\rangle\frac{\partial}{\partial z}G^F(z;\tilde{\xi})d\tilde{\xi} \tag{D.7}$$

Substituting (D.5)-(D.7) into (D.2) leads to

$$\left\langle\overline{v_z^{st}{}'(z)v_z^{dy}{}'(\xi,\tau)}\right\rangle\approx\frac{\mathrm{N_g}}{\phi}\left\{\begin{array}{l}-\left\langle\overline{Y(z)C'(\xi,\tau)}\right\rangle\\-\int_0^H\int_0^H\frac{\partial^2}{\partial\tilde{\xi}\partial\xi}\left\langle\overline{Y(\tilde{\xi})C'(\xi,\tau)}\right\rangle\frac{\partial}{\partial z}G^F(z;\tilde{\xi})\frac{\partial}{\partial\xi}G^F(\xi;\hat{\xi})d\xi d\tilde{\xi}\\+\int_0^H\frac{\partial}{\partial\tilde{\xi}}\left\langle\overline{Y(\tilde{\xi})C'(\xi,\tau)}\right\rangle\frac{\partial}{\partial z}G^F(z;\tilde{\xi})d\tilde{\xi}+\\+\int_0^H\frac{\partial}{\partial\hat{\xi}}\left\langle\overline{Y(z)C'(\hat{\xi},\tau)}\right\rangle\frac{\partial}{\partial\xi}G^F(\xi;\hat{\xi})d\hat{\xi}\end{array}\right\}. \tag{D.8}$$

Equation (D.8) indicates that $\left\langle\overline{v_z^{st}{}'(z)v_z^{dy}{}'(\xi,\tau)}\right\rangle$ depends sub-linearly on $\mathrm{N_g}/\phi$ and is a function of the cross-covariance $\left\langle\overline{Y(z)C'(\xi,\tau)}\right\rangle$.

Following a similar procedure, one can then write $\left\langle\overline{v_z^{dy}{}'(z,t)v_z^{st}{}'(\xi)}\right\rangle$, $\left\langle\overline{v_z^{dy}{}'(z,t)v_z^{dy}{}'(\xi,\tau)}\right\rangle$ and $\left\langle\overline{v_z^{st}{}'(z)v_z^{st}{}'(\xi)}\right\rangle$ respectively as

$$\left\langle\overline{v_z^{dy}{}'(z,t)v_z^{st}{}'(\xi)}\right\rangle\approx\frac{\mathrm{N_g}}{\phi}\left\{\begin{array}{l}-<\overline{C'(z,t)Y(\xi)}>\\-\int_0^H\int_0^H\frac{\partial^2}{\partial\tilde{\xi}\partial\xi}\left\langle\overline{Y(\tilde{\xi})C'(\xi,t)}\right\rangle\frac{\partial}{\partial z}G^F(z;\xi)\frac{\partial}{\partial\xi}G^F(\xi;\tilde{\xi})d\xi d\tilde{\xi}\\+\int_0^H\frac{\partial}{\partial\hat{\xi}}\left\langle\overline{C'(z,t)Y(\hat{\xi})}\right\rangle\frac{\partial}{\partial\xi}G^F(\xi;\hat{\xi})d\hat{\xi}\\+\int_0^H\frac{\partial}{\partial\hat{\xi}}\left\langle\overline{Y(\xi)C'(\hat{\xi},t)}\right\rangle\frac{\partial}{\partial z}G^F(z;\hat{\xi})d\hat{\xi}\end{array}\right\} \tag{D.9}$$

$$\left\langle \overline{v_z^{dy}{}'(z,t)v_z^{dy}{}'(\xi,\tau)} \right\rangle \approx \left(\frac{\mathrm{N_g}}{\phi}\right)^2 \left\{ \begin{array}{l} \left\langle \overline{C'(z,t)C'(\xi,\tau)} \right\rangle \\ +\int_0^H \int_0^H \frac{\partial^2}{\partial\tilde{\xi}\partial\hat{\xi}} \left\langle \overline{C'(\hat{\xi},t)C'(\tilde{\xi},\tau)} \right\rangle \frac{\partial}{\partial z} G^F(z;\hat{\xi}) \frac{\partial}{\partial \xi} G^F(\xi;\tilde{\xi}) d\tilde{\xi} d\hat{\xi} \\ -\int_0^H \frac{\partial}{\partial \hat{\xi}} \left\langle \overline{C'(\hat{\xi},t)C'(\xi,\tau)} \right\rangle \frac{\partial}{\partial z} G^F(z;\hat{\xi}) d\hat{\xi} \\ -\int_0^H \frac{\partial}{\partial \hat{\xi}} \left\langle \overline{C'(\hat{\xi},\tau)C'(z,t)} \right\rangle \frac{\partial}{\partial \xi} G^F(\xi;\hat{\xi}) d\hat{\xi} \end{array} \right\} \quad \text{(D.10)}$$

$$\left\langle \overline{v_z^{st}{}'(z)v_z^{st}{}'(\xi)} \right\rangle \approx \left\{ \begin{array}{l} \left\langle \overline{Y(z)Y(z)} \right\rangle \\ +\int_0^H \int_0^H \frac{\partial^2}{\partial\hat{\xi}\partial\tilde{\xi}} \left\langle Y(\hat{\xi})Y(\tilde{\xi}) \right\rangle \frac{\partial}{\partial \xi} G^F(\xi;\hat{\xi}) \frac{\partial}{\partial z} G^F(z;\tilde{\xi}) d\hat{\xi} d\tilde{\xi} - \\ -\int_0^H \frac{\partial}{\partial \hat{\xi}} \left\langle \overline{Y(z)Y(\hat{\xi})} \right\rangle \frac{\partial}{\partial \xi} G^F(\xi;\hat{\xi}) d\hat{\xi} - \\ -\int_0^H \frac{\partial}{\partial \hat{\xi}} \left\langle Y(\xi)Y(\hat{\xi}) \right\rangle \frac{\partial}{\partial z} G^F(z;\hat{\xi}) d\hat{\xi} \end{array} \right\} \quad \text{(D.11)}$$

Equation (D.10) shows that $\left\langle \overline{v_z^{dy}{}'(z,t)v_z^{dy}{}'(\xi,\tau)} \right\rangle$ depends sub-linearly on $\left(\mathrm{N_g}/\phi\right)^2$ and is a function of $\left\langle \overline{C'(z,t)C'(\xi,\tau)} \right\rangle$, i.e., the horizontal spatial mean of concentration covariance. It is also seen that $\left\langle \overline{v_z^{st}{}'(z)v_z^{st}{}'(\xi)} \right\rangle$ is a function of the covariance of Y.

We now introduce the following notation

$$\begin{aligned} \left\langle \overline{v'_z(z,t)v'_z(\xi,\tau)} \right\rangle = \mathbf{A}\left\{ \left\langle \overline{Y(z)Y(\xi)} \right\rangle \right\} + \frac{\mathrm{N_g}}{\phi} \mathbf{B}\left\{ \left\langle \overline{Y(z)C'(\xi,\tau)} \right\rangle \right\} + \\ + \frac{\mathrm{N_g}}{\phi} \mathbf{C}\left\{ \left\langle \overline{C'(z,t)Y(\xi)} \right\rangle \right\} + \frac{\mathrm{N_g^2}}{\phi^2} \mathbf{D}\left\{ \left\langle \overline{C'(z,t)C'(\xi,\tau)} \right\rangle \right\} \end{aligned} \quad \text{(D.12)}$$

where operators $\mathbf{A}\{\ \}$, $\mathbf{B}\{\ \}$, $\mathbf{C}\{\ \}$, $\mathbf{D}\{\ \}$ are respectively defined by the terms in parenthesis appearing at the right hand side of (D.11), (D.8), (D.9) and (D.10). As highlighted by (D.12), one needs to derive the equations satisfied by the cross-covariances $\left\langle \overline{C'(z,t)Y(\xi)} \right\rangle$ and $\left\langle \overline{C'(z,t)C'(\xi,\tau)} \right\rangle$ to determine $\left\langle \overline{v'_z(z,t)v'_z(\xi,\tau)} \right\rangle$. These expressions are respectively derived in Appendices E and F.

Appendix E. Cross covariance between permeability and concentration

Here we derive the horizontal spatial mean of the cross-covariance between the log-permeability and concentration, i.e., $\left\langle \overline{Y(z)C'(\xi,\tau)} \right\rangle$. Multiplying (A.8) by $Y(y,z)$, applying (13) and the ensemble

averaging operator, making use of (A.10) and disregarding products of fluctuations larger than two yields

$$\begin{aligned}\left\langle \overline{Y(z)C'(\xi,\tau)} \right\rangle &= \frac{1}{W}\int_0^W \left\langle Y(z,y)C'(\eta=y,\xi,\tau)\right\rangle dy \\ &= -\frac{1}{W}\int_0^t\int_0^H\int_0^W \left\langle Y(z,y)v_z'(y,\hat{\xi},\hat{\tau})\right\rangle \frac{\partial}{\partial\hat{\xi}}\left\langle \overline{C}(\hat{\xi},\hat{\tau})\right\rangle G_z^T(\xi,\tau,\hat{\xi},\hat{\tau})\,dy\,d\hat{\xi}\,d\hat{\tau} \\ &= -\int_0^t\int_0^H \left\langle \overline{Y(z)v_z'(\hat{\xi},\hat{\tau})}\right\rangle G_z^T(\xi,\tau,\hat{\xi},\hat{\tau})\frac{\partial}{\partial\hat{\xi}}\left\langle \overline{C}(\hat{\xi},\hat{\tau})\right\rangle d\hat{\xi}\,d\hat{\tau}.\end{aligned} \tag{E.1}$$

Recalling (C.5), equation (E.1) becomes

$$\begin{aligned}\left\langle \overline{Y(z)C'(\xi,\tau)} \right\rangle = -\int_0^t\int_0^H \frac{\partial}{\partial\hat{\xi}}\left\langle \overline{C}(\hat{\xi},\hat{\tau})\right\rangle G_z^T(\xi,\tau,\hat{\xi},\hat{\tau}) \\ \left\{\left\langle \overline{Y(z)Y(\hat{\xi})}\right\rangle - \frac{1}{\phi}\frac{\partial}{\partial\hat{\xi}}\left\langle \overline{Y(z)p^{st}'(\hat{\xi})}\right\rangle - \frac{\mathrm{N_g}}{\phi}\left\langle \overline{Y(z)C'(\hat{\xi},\hat{\tau})}\right\rangle - \frac{1}{\phi}\frac{\partial}{\partial\hat{\xi}}\left\langle \overline{Y(z)p^{dy}'(\hat{\xi},\hat{\tau})}\right\rangle\right\} d\hat{\xi}\,d\hat{\tau}\end{aligned} . \tag{E.2}$$

A numerically analysis of (E.2) (details not shown) allows recognizing that it is possible to disregard the last term on the right hand side of (E.2) for the test cases considered in this work. Introducing the operator $\mathbf{F}\{\ \}$ defined as

$$\mathbf{F}\left\{\Theta(z;\xi,\hat{\tau})\right\} = -\int_0^t\int_0^H \Theta(z;\xi,\hat{\tau})G_z^T(\xi,\tau,\hat{\xi},\hat{\tau})\frac{\partial}{\partial\hat{\xi}}\left\langle \overline{C}(\hat{\xi},\hat{\tau})\right\rangle d\xi\,d\hat{\tau}\,, \tag{E.3}$$

allows rewriting (E.2) as

$$\left\langle \overline{Y(z)C'(\xi,\tau)} \right\rangle + \frac{\mathrm{N_g}}{\phi}\mathbf{F}\left\{\left\langle \overline{Y(z)C'(\hat{\xi},\hat{\tau})}\right\rangle\right\} = \mathbf{F}\left\{\left\langle \overline{Y(z)Y(\hat{\xi})}\right\rangle\right\} - \frac{1}{\phi}\mathbf{F}\left\{\frac{\partial}{\partial\hat{\xi}}\left\langle \overline{Y(z)p^{st}'(\hat{\xi})}\right\rangle\right\}. \tag{E.4}$$

Equation (E.4) provides the link amongst $\left\langle \overline{Y(z)C'(\xi,\tau)} \right\rangle$ and (*i*) the covariance of *Y*, i.e., $\left\langle \overline{Y(z)Y(\xi)} \right\rangle$, and (*ii*) the cross-covariance between *stationary* pressure and permeability, i.e. $\left\langle \overline{Y(z)p^{st}'(\xi)} \right\rangle$.

Introducing the dimensionless hydraulic head $h = p^{st}/g\rho_f + z$ ($v_{BC}^*\, g = \sqrt{\tilde{k}^*}\, g^*/{v_{BC}^*}^2$ being the dimensionless gravity), allows rewriting (E.4) as

$$\left\langle \overline{Y(z)C'(\xi,\tau)} \right\rangle = \mathbf{F}\left\{\left\langle \overline{Y(z)Y(\hat{\xi})}\right\rangle\right\} - \frac{g\rho_f}{\phi}\mathbf{F}\left\{\frac{\partial}{\partial\hat{\xi}}\left\langle \overline{Y(z)h'(\hat{\xi})}\right\rangle\right\} - \frac{\mathrm{N_g}}{\phi}\mathbf{F}\left\{\left\langle \overline{Y(z)C'(\hat{\xi},\hat{\tau})}\right\rangle\right\}, \tag{E.5}$$

where $\left\langle \overline{Y(z)h'(\hat{\xi})} \right\rangle$ is the cross-covariance between log-permeability and hydraulic head for the constant density case. The last term on right hand side of (E.5) embeds the stabilizing buoyancy effects which reduce the correlation between permeability and concentration.

Appendix F. Concentration Covariance

Here we derive the equation satisfied by the horizontal spatial mean of concentration covariance, $\left\langle \overline{C'(z,t)C'(\xi,\tau)} \right\rangle$. Multiplying (A.8) by $C'(\eta,\xi,\tau)$, taking the ensemble mean operator, making use of (A.10) and neglecting terms involving power of fluctuations larger than two yields

$$\left\langle C'(z,y,t)C'(\xi,\eta,\tau) \right\rangle = -\int_0^H \int_0^t \left\langle v_z'(\hat{\eta}=\eta,\hat{\xi},\hat{\tau})C'(z,y,t) \right\rangle \frac{\partial}{\partial \hat{\xi}} \left\langle \overline{C}(\hat{\xi},\hat{\tau}) \right\rangle G_z^T(\xi,\tau,\hat{\xi},\hat{\tau}) d\hat{\xi} d\hat{\tau} \,. \tag{F.1}$$

The term $\left\langle \overline{C'(z,t)C'(\xi,\tau)} \right\rangle$ is defined as

$$\left\langle \overline{C'(z,t)C'(\xi,\tau)} \right\rangle = \frac{1}{W} \int_0^W \left\langle C'(\eta=y,\xi,\tau)C'(z,y,t) \right\rangle dy \,. \tag{F.2}$$

Recalling (C.5), (F.2) becomes

$$\left\langle \overline{C'(z,t)C'(\xi,\tau)} \right\rangle = -\int_0^H \int_0^t \frac{\partial}{\partial \hat{\xi}} \left\langle \overline{C}(\hat{\xi},\hat{\tau}) \right\rangle G_z^T(\xi,\tau,\hat{\xi},\hat{\tau})$$
$$\left(\left\langle \overline{Y(\hat{\xi})C'(z,t)} \right\rangle - \frac{1}{\phi} \frac{\partial}{\partial \hat{\xi}} \left\langle \overline{C'(z,t)p^{st}'(\hat{\xi})} \right\rangle - \frac{\mathrm{N_g}}{\phi} \left\langle \overline{C'(z,t)C'(\hat{\xi},\hat{\tau})} \right\rangle - \frac{1}{\phi} \frac{\partial}{\partial \hat{\xi}} \left\langle \overline{C'(z,t)p^{dy}'(\hat{\xi},\hat{\tau})} \right\rangle \right) d\hat{\xi} d\hat{\tau}$$

. (F.3)

A numerically analysis of (F.3) (details not shown) allows recognizing that it is possible to disregard the last term on the right hand side of (F.3) for the test cases considered in this work. Introducing the operator $\mathbf{H}\{\ \}$ defined as

$$\mathbf{H}\left\{ \Theta(z,t;\xi,\hat{\tau}) \right\} = -\int_0^t \int_0^H \Theta(z,t;\xi,\hat{\tau}) G_z^T(\xi,\tau,\hat{\xi},\hat{\tau}) \frac{\partial}{\partial \hat{\xi}} \left\langle \overline{C}(\hat{\xi},\hat{\tau}) \right\rangle d\xi d\hat{\tau} \,, \tag{F.4}$$

allows rewriting (F.3) as

$$\left\langle \overline{C'(z,t)C'(\xi,\tau)} \right\rangle = \mathbf{H}\left\{ \left\langle \overline{Y(\hat{\xi})C'(z,t)} \right\rangle \right\} - \frac{1}{\phi} \mathbf{H}\left\{ \frac{\partial}{\partial \hat{\xi}} \left\langle \overline{C'(z,t)p^{st}'(\hat{\xi})} \right\rangle \right\} - \frac{\mathrm{N_g}}{\phi} \mathbf{H}\left\{ \left\langle \overline{C'(z,t)C'(\hat{\xi},\hat{\tau})} \right\rangle \right\} \tag{F.5}$$

The last term in (F.5) represents the impact of the stabilizing buoyancy effects and leads to a reduction in the concentration variance as discussed in Section 4.3. Finally, making use of (C.8) allows rewriting (F.5) as

$$\left\langle \overline{C'(z,t)C'(\xi,\tau)} \right\rangle + \frac{\mathrm{N_g}}{\phi} \mathbf{H}\left\{ \left\langle \overline{C'(z,t)C'(\hat{\xi},\hat{\tau})} \right\rangle \right\} =$$
$$\mathbf{H}\left\{ \left\langle \overline{Y(\hat{\xi})C'(z,t)} \right\rangle \right\} - \mathbf{H}\left\{ \frac{\partial}{\partial \hat{\xi}} \int_0^H \frac{\partial}{\partial \tilde{\xi}} \left\langle \overline{C'(z,t)Y(\tilde{\xi})} \right\rangle G^F(\hat{\xi};\tilde{\xi}) d\tilde{\xi} \right\} \,. \tag{F.6}$$

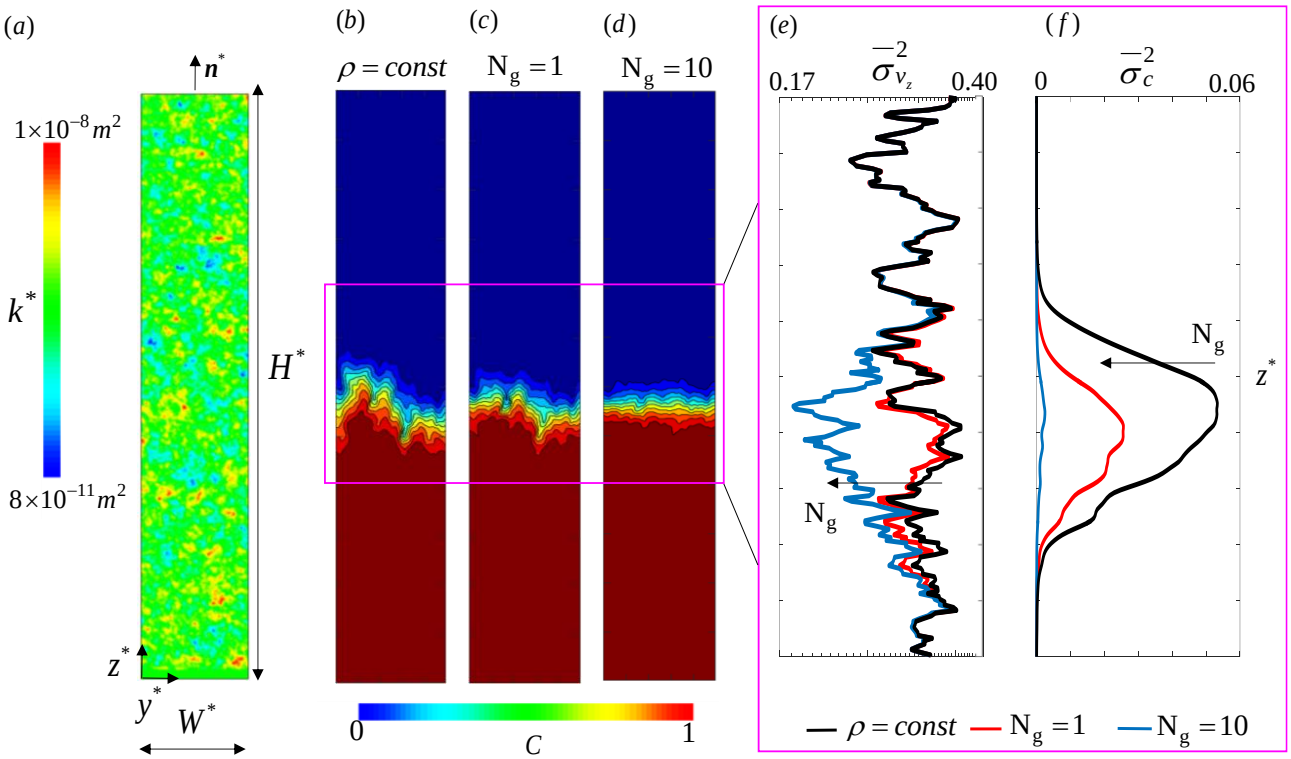

Fig. 1. (*a*) Flow and transport problem set-up and colorized image of the permeability field for $\sigma_Y^2 = 0.5$. Sample contour plots of normalized concentration for (*b*) constant density, (*c*) N_g = 1 and (*d*) N_g =10, with $N_g = \Delta\rho^* \tilde{k}^* g^* / (\mu^* v_{BC}^*)$. Magnification at solute front of the spatial variance of (*e*) vertical velocity, i.e., $\overline{\sigma}^2_{v_z}$, and (*f*) of concentration, i.e., $\overline{\sigma}^2_{C}$.

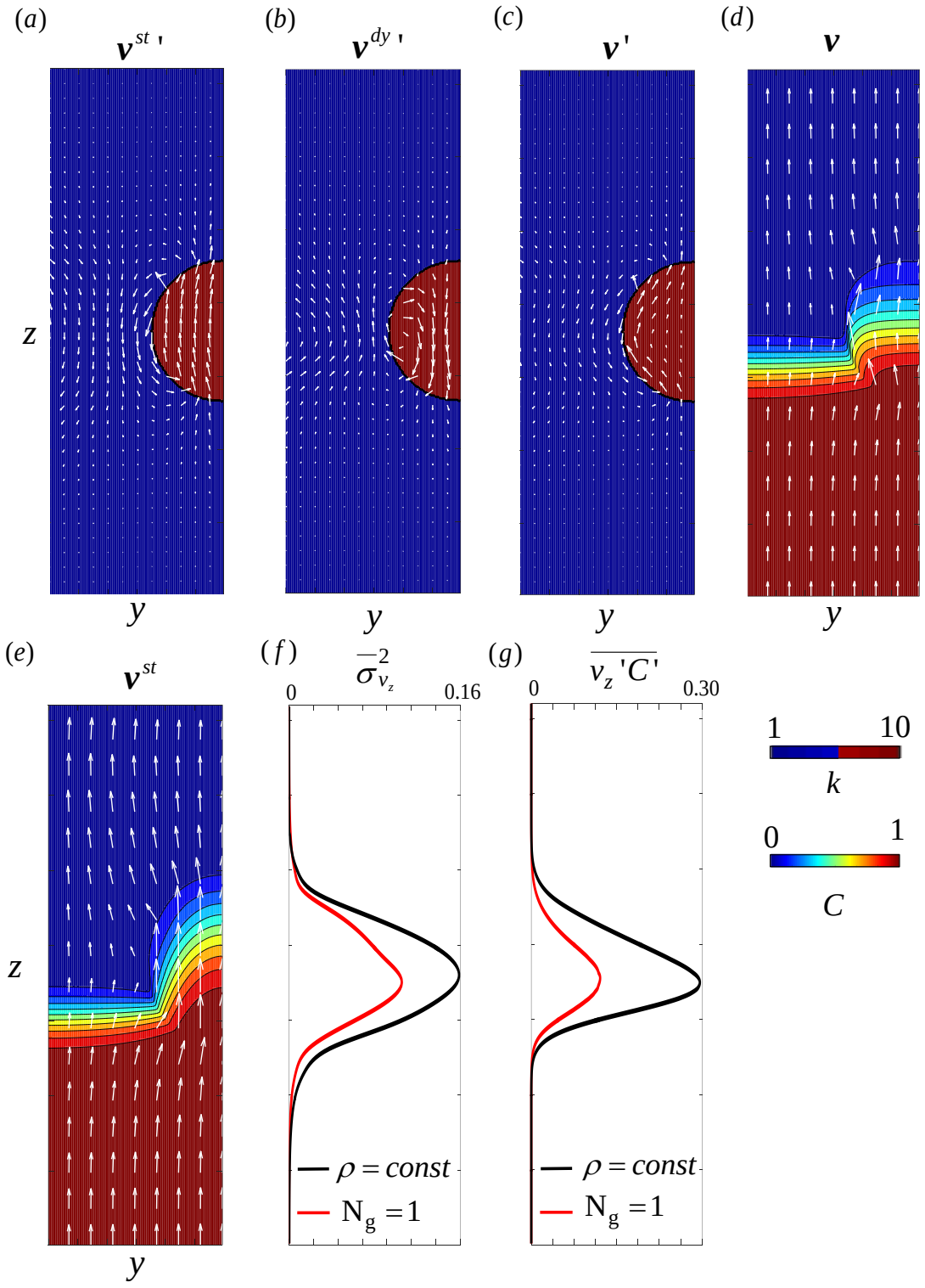

Fig. 2. Examples of (*a*) $\boldsymbol{v}^{'st}$, (*b*) $\boldsymbol{v}^{'dy}$ and (*c*) $\boldsymbol{v}'$ for the variable density flow problem. The underlying $\boldsymbol{k}$ field is also depicted. Velocity, $\boldsymbol{v}$, and concentration, C (depicted as color scale), for (*d*) variable and (*e*) constant density. Vertical distribution of (*f*) variance of vertical velocity, $\overline{\sigma}^{2}_{v_z}$, and (*g*) *single realization* dispersive flux (19), i.e., $\overline{v_z'C'}$, for the tracer (red curve) and variable density (black curve) case. All of the results have been evaluated at t = 664.

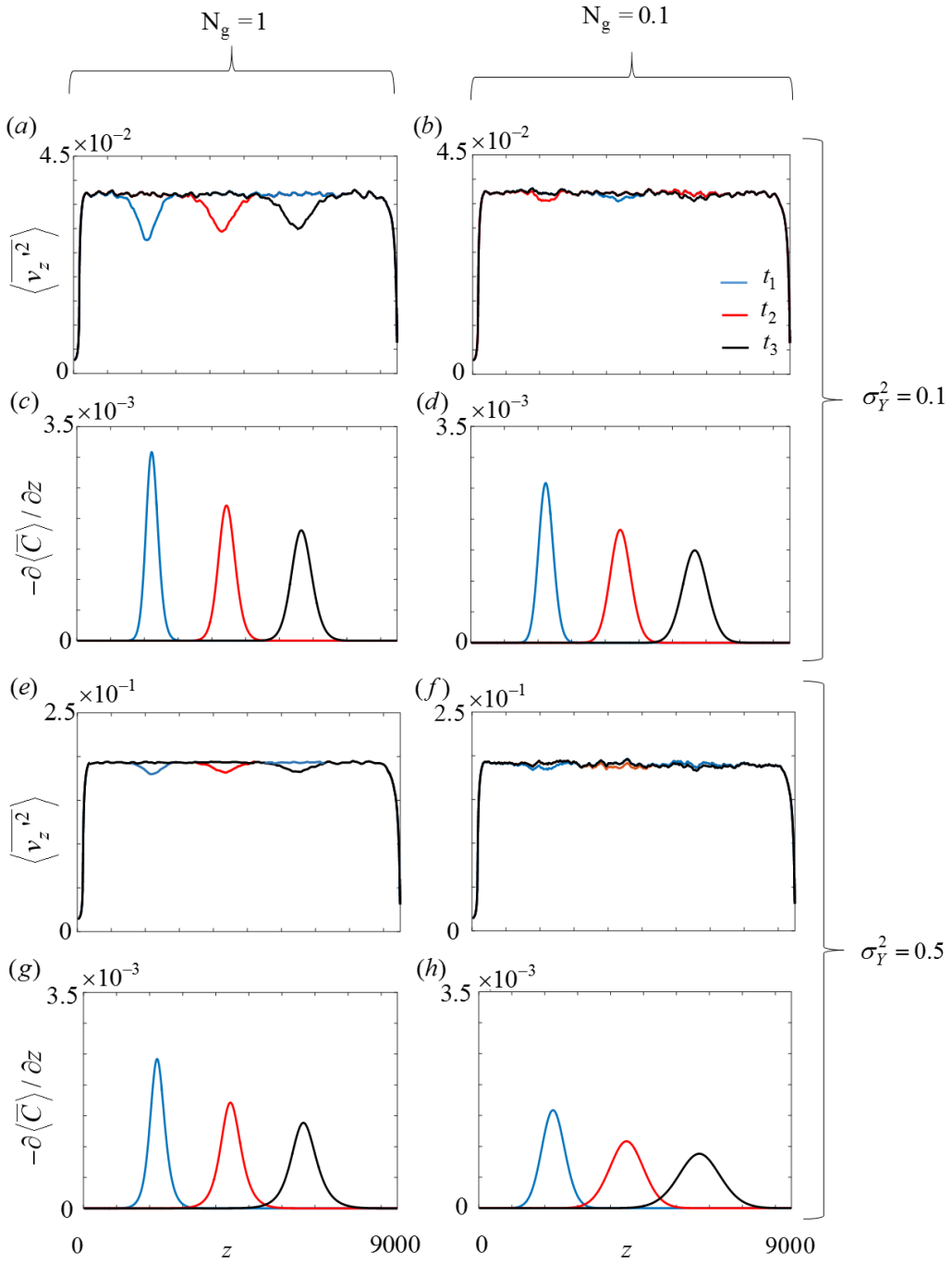

Fig. 3. Section-averaged vertical velocity variance, $\langle \overline{v_z}'^2 \rangle$, and (negative) gradient of ensemble concentration ($-\partial \langle \overline{C} \rangle / \partial z$) for (*a*), (*c*) $\sigma_Y^2 = 0.1$ and $N_g = 1$; (*b*), (*d*) $\sigma_Y^2 = 0.1$ and $N_g = 0.1$; (*e*), (*g*) $\sigma_Y^2 = 0.5$ and $N_g = 1$; (*f*), (*h*) $\sigma_Y^2 = 0.5$ and $N_g = 0.1$. Results are evaluated at dimensionless times $t_1 < t_2 < t_3$.

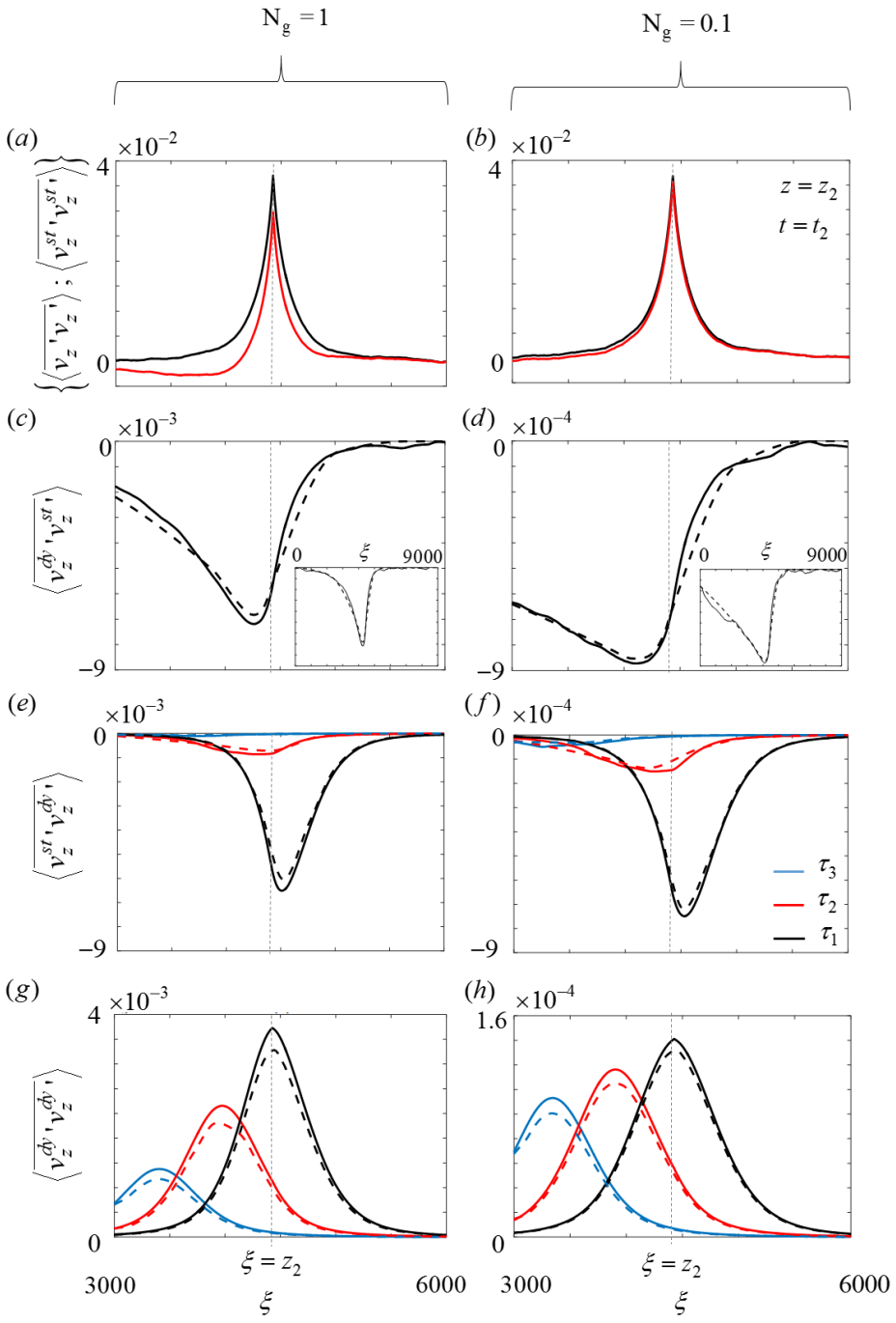

Fig. 4. Section-averaged vertical velocity covariance components for $z = z_2 = 4.27\times10^3$: (*a*, *b*) $\left\langle \overline{v'_z(z,t)v'_z(\xi,\tau)} \right\rangle$ (red curve) and $\left\langle \overline{v_z^{st}(z)v_z^{st}(\xi)} \right\rangle$ (black curve); (*c*, *d*) $\left\langle \overline{v_z^{dy}(z,t)v_z^{st}(\xi)} \right\rangle$ (insets show the entire vertical domain); (*e*, *f*) $\left\langle \overline{v_z^{st}(z)v_z^{dy}(\xi,\tau)} \right\rangle$; (*g*, *h*) $\left\langle \overline{v_z^{dy}(z,t)v_z^{dy}(\xi,\tau)} \right\rangle$ versus ξ for $\sigma_Y^2 = 0.1$ and $N_g = 1$ (left column) or $N_g = 0.1$ (right column). In (*a*)-(*d*) and (*g*)-(*h*) $t = t_2 = 4.4\times10^3$; in (*e*)-(*h*) $\tau_1 = 4.4\times10^3$, $\tau_2 = 3.9\times10^3$, $\tau_3 = 3.3\times10^3$. Numerical Monte Carlo and semi-analytical solutions are depicted as solid and dashed curves, respectively.

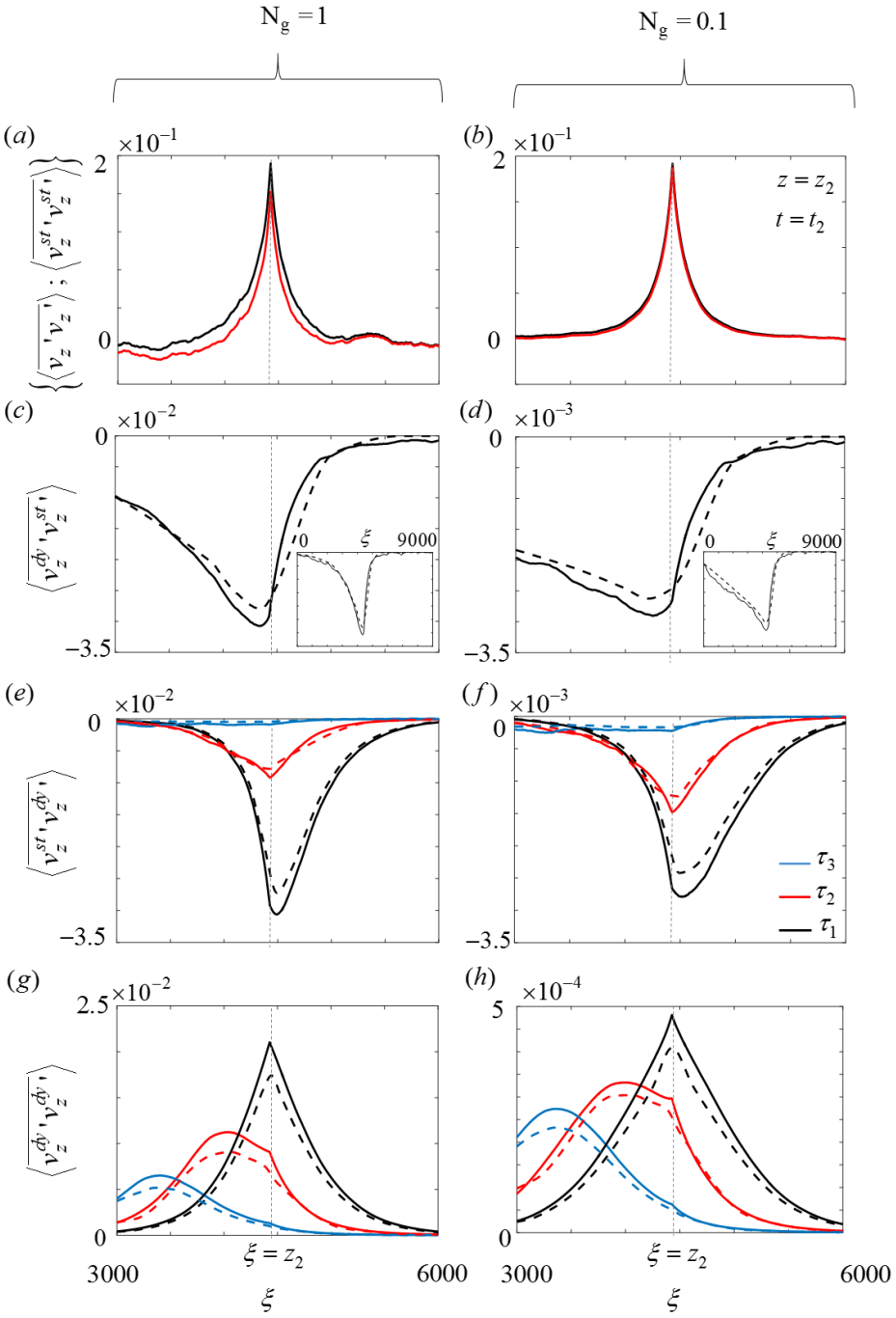

Fig. 5. Section-averaged vertical velocity covariance components for $z = z_2 = 4.27\times10^3$: (*a*, *b*) $\left\langle \overline{v'_z(z,t)v'_z(\xi,\tau)} \right\rangle$ (red curve) and, $\left\langle \overline{v_z^{st}{}'(z)v_z^{st}{}'(\xi)} \right\rangle$ (black curve); (*c*, *d*) $\left\langle \overline{v_z^{dy}{}'(z,t)v_z^{st}{}'(\xi)} \right\rangle$ (insets show the entire vertical domain); (*e*, *f*) $\left\langle \overline{v_z^{st}{}'(z)v_z^{dy}{}'(\xi,\tau)} \right\rangle$; (*g*, *h*) $\left\langle \overline{v_z^{dy}{}'(z,t)v_z^{dy}{}'(\xi,\tau)} \right\rangle$ versus ξ for $\sigma_Y^2 = 0.5$ and $N_g = 1$ (left column) or $N_g = 0.1$ (right column).). In (*a*)-(*d*) and (*g*)-(*h*) $t = t_2 = 4.4\times10^3$; in (*e*)-(*h*) $\tau_1 = 4.4\times10^3$, $\tau_2 = 3.9\times10^3$, $\tau_3 = 3.3\times10^3$. Numerical Monte Carlo and semi-analytical solutions are depicted as solid and dashed curves, respectively.

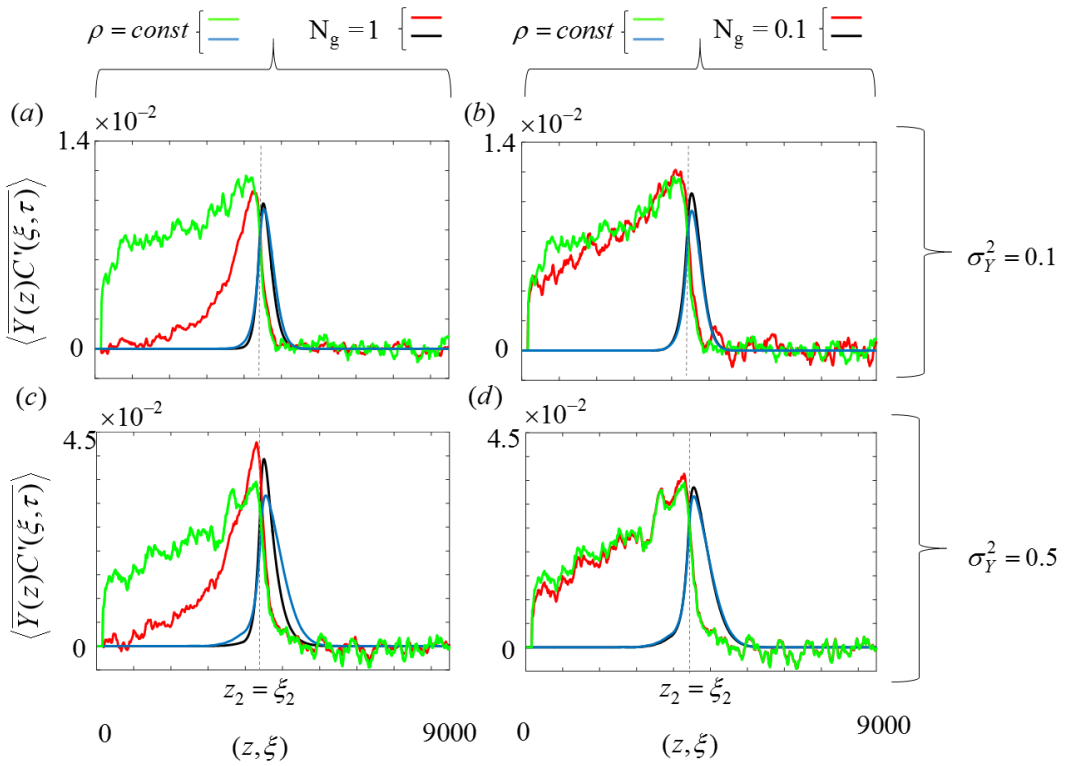

Fig. 6. Section-averaged log-permeability and concentration cross-covariance, $\left\langle \overline{Y(z)C'(\xi,\tau)} \right\rangle$, versus ξ when $z = z_2 = 4.27\times10^3$ (black curves) or versus z when $\xi = \xi_2 = 4.27\times10^3$ (red curves) at time $\tau = t_2 = 4.4\times10^3$ for $\sigma_Y^2 = 0.1$, 0.5 and (*a*,*c*) $N_g = 1$, or (*b*,*d*) $N_g = 0.1$. The results obtained for the tracer case (i.e., $\rho = cost$) are also depicted for $\left\langle \overline{Y(z_2)C'(\xi,\tau)} \right\rangle$ (blues curves) and $\left\langle \overline{Y(z)C'(\xi_2,\tau)} \right\rangle$ (green curves).

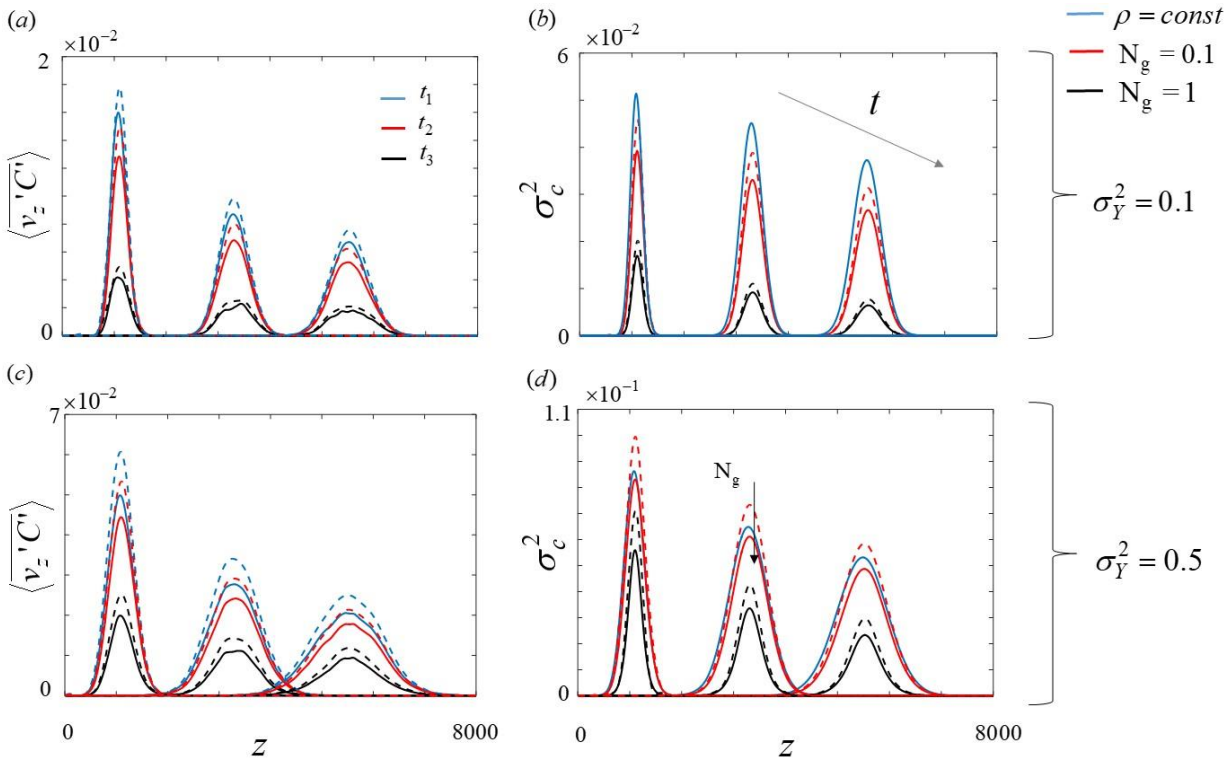

Fig. 7. Section-averaged ensemble dispersive flux, $\left\langle \overline{v_z'(z,t)C'(z,t)} \right\rangle$, and concentration variance, $\sigma_c^2(z,t) = \left\langle \overline{C'(z,t)^2} \right\rangle$, for $N_g = 1$, (black curves), $N_g = 0.1$, (red curves), $\rho = cost$, (blue curves), (*a*)-(*b*) for $\sigma_Y^2 = 0.1$ and (*c*)- (*d*) for $\sigma_Y^2 = 0.5$. Numerical Monte Carlo and semi-analytical solutions of (25) (for $\left\langle \overline{v_z'C'} \right\rangle$) and (F.6) (for $\sigma_c^2(z,t)$) are depicted as solid and dashed curves, respectively. Results are evaluated at dimensionless times $t_1 < t_2 < t_3$.